

**Time-Multipatch Discontinuous
Galerkin Space-Time Isogeometric
Analysis of Parabolic Evolution
Problems**

Christoph Hofer Langer Ulrich Neumüller Martin
Toulopoulos Ioannis

DK-Report No. 2017-05

08 2017

A-4040 LINZ, ALTENBERGERSTRASSE 69, AUSTRIA

Supported by

Austrian Science Fund (FWF)

Upper Austria

Editorial Board: Bruno Buchberger
Bert Jüttler
Ulrich Langer
Manuel Kauers
Esther Klann
Peter Paule
Clemens Pechstein
Veronika Pillwein
Silviu Radu
Ronny Ramlau
Josef Schicho
Wolfgang Schreiner
Franz Winkler
Walter Zulehner

Managing Editor: Silviu Radu

Communicated by: Veronika Pillwein
Bert Jüttler

DK sponsors:

- **Johannes Kepler University Linz (JKU)**
- **Austrian Science Fund (FWF)**
- **Upper Austria**

Time-Multipatch Discontinuous Galerkin Space-Time Isogeometric Analysis of Parabolic Evolution Problems

Christoph Hofer¹, Ulrich Langer^{1,2,3}, Martin Neumüller², and Ioannis Touloupoulos³

1 Doctoral Program “Computational Mathematics”
Johannes Kepler University,

2 Institute of Computational Mathematics,
Johannes Kepler University,

3 Johann Radon Institute for Computational and Applied Mathematics,
Austrian Academy of Sciences

Altenbergerstr. 69, A-4040 Linz, Austria,

christoph.hofer@dk-compmath.jku.at

ulanger@numa.uni-linz.ac.at

neumueller@numa.uni-linz.ac.at

ioannis.touloupoulos@ricam.oeaw.ac.at

Abstract. In this paper, we present a new time-multipatch discontinuous Galerkin Isogeometric Analysis (IgA) technology for solving parabolic initial-boundary problems in space and time simultaneously. We prove coercivity of the discrete IgA problem with respect to a suitably chosen norm that together with boundedness, consistency and approximation results yields a priori discretization error estimates in this norm. Furthermore, we provide efficient parallel generation and parallel multigrid solution technologies, and present first numerical results on massively parallel computers.

Key words: Parabolic initial-boundary value problems, Space-time Isogeometric Analysis, Time discontinuous Galerkin methods, Space-time multigrid solvers.

1 Introduction

Fully discrete schemes for parabolic initial-boundary value problems (IBVP) are usually derived by discretizing either first in space by means of some spatial discretization method like the finite element method and then in time by some time-stepping method or vice versa. The former methods are called vertical methods of lines [58], the latter horizontal methods of lines or Rothe’s methods [33]. Time-stepping methods are sequential in time. To overcome this curse of sequentiality on massively parallel computers, one needs some smart ideas for the parallelization in time. Time parallel methods have a long and exciting history that can be found in the very nice paper [18] on *50 Years of Time Parallel Time Integration*. Space-time finite element methods for parabolic and hyperbolic Partial Differential Equations (PDEs) go back to the 80s and 90s of the last century [27, 28, 26, 3, 4, 20], and enjoy a real revival during the last couple of years due to the availability of massively parallel computers with thousands or hundred thousands of cores, see, e.g., [49], [44], [1], [6], [43], [41], [60], [51], [2], [50], [5], [38], [59] for some recent mathematical papers related to parabolic problems. Moreover, there are several recent papers on the efficient use of various space-time methods for solving exciting engineering problems involving moving computational spatial domains or / and interfaces see, e.g., [8], [56], [53], [54], [55], [57], [29], [30] and the references therein.

In [35], we were inspired by looking at the time variable t in a parabolic problem as just another variable, say, x_{d+1} if x_1, \dots, x_d are the spatial variable, and at the time derivative as a strong convection in the direction x_{d+1} that can numerically be treated in a stable way by special discretization techniques known from convection dominated elliptic convection-diffusion problems, see, e.g., [52]. The most popular stabilizing method is the Streamline-Upwind Petrov-Galerkin (SUPG) method introduced in [24]. We have used time-upwind test functions to construct stable single-patch space-time Isogeometric Analysis (IgA) schemes the discrete bilinear form of which is coercive (elliptic) on the IgA space with respect to a suitably chosen mesh-dependent energy

norm. This coercivity (ellipticity) property together with a corresponding boundedness property, consistency and approximation results for the IgA spaces yields the corresponding a priori discretization error estimate. A posteriori error estimates that can be used for space-time adaptivity are derived in [34].

IgA was introduced in [25] as a new discretization methodology for PDE-based models. The core idea of IgA is to use the same smooth and high-order superior finite dimensional B-spline or NURBS spaces for parametrizing the computational domain and for approximating the solution of the PDE model under consideration. IgA approaches have successfully been applied to the solution of a wide range of linear and nonlinear problems. Their benefits have been highlighted in many publications, see, e.g., the monograph [13], the survey paper [10] and the references therein. Although results related to the approximate properties of B-splines and their use for discretizing PDEs existed before, see, e.g., [48] and [23], the theoretical frame involving the parametrization mappings has been started in [7], where the authors studied the approximation properties of B-splines (NURBS) in bent Sobolev spaces. In particular, they showed that the mapped B-splines have the same approximation order in terms of the mesh size h as the piecewise polynomials of the same degree p , see also [9], [11], [10] for the generalization of these approximation results.

In this paper, we generalize the results of [35] from the single-patch to time-multipatch discontinuous Galerkin (dG) space-time IgA schemes. As in [35], we consider the linear parabolic IBVP, find $u : \bar{Q} \rightarrow \mathbb{R}$ such that

$$\partial_t u - \Delta u = f \text{ in } Q, \quad u = 0 \text{ on } \Sigma, \quad \text{and } u = u_0 \text{ on } \Sigma_0, \quad (1.1)$$

as a typical parabolic model problem posed in the space-time cylinder $\bar{Q} = \bar{\Omega} \times [0, T] = Q \cup \Sigma \cup \bar{\Sigma}_0 \cup \bar{\Sigma}_T$, where ∂_t denotes the partial time derivative, Δ is the Laplace operator, f is a given source function, u_0 are the given initial data, T is the final time, $Q = \Omega \times (0, T)$, $\Sigma = \partial\Omega \times (0, T)$, $\Sigma_0 := \Omega \times \{0\}$, $\Sigma_T := \Omega \times \{T\}$, and $\Omega \subset \mathbb{R}^d$ ($d = 1, 2, 3$) denotes the spatial computational domain with the boundary $\partial\Omega$. The spatial domain Ω is supposed to have a singlepatch NURBS representation as is used in CAD [47]. More precisely, the space-time cylinder $\bar{Q} = \cup_{n=1}^N \bar{Q}_n$ is composed of N subcylinders (patches or time slices) $Q_n = \Omega \times (t_{n-1}, t_n)$, $n = 1, \dots, N$, where $0 = t_0 < t_1 < \dots < t_N = T$ is some subdivision of time interval $[0, T]$. The time faces between the time patches are denoted by $\bar{\Sigma}_n = \bar{Q}_{n+1} \cap \bar{Q}_n = \bar{\Omega} \times \{t_n\}$, where $\Sigma_N = \Sigma_T$. Every space-time patch $Q_n = \Phi_n(\hat{Q})$ in the physical domain Q can be represented as the image of the parameter domain $\hat{Q} = (0, 1)^{d+1}$ by means of a sufficiently regular IgA (B-Spline, NURBS etc.) map $\Phi_n : \hat{Q} \rightarrow Q_n$ that can be easily constructed from the spatial IgA map from $\hat{\Omega} = (0, 1)^d$ to Ω . In particular, each Q_n can have its own mesh defined according to the characteristics of the problem. Therefore, the IgA spaces V_{h0} , which we are going to use, are smooth in each time patch Q_n , but discontinuous across the time faces Σ_n . For stabilizing the time discretization, the method incorporates ideas of streamline diffusion methodology. The continuity of the patch-wise defined approximate solutions is ensured by introducing simple ‘‘up-wind’’ jump terms across the interfaces. The jump terms do not include normal fluxes. This simplifies the error analysis. Moreover, the whole method can easily be materialized on a parallel platform. We develop a thoroughly theoretical study of the method. After defining the appropriate discontinuous B-spline spaces and after defining the related discrete norm, we prove that the produced discrete bilinear form is coercive (elliptic) with respect to this norm. This property ensures uniqueness and existence of the IgA solution. Based on this ellipticity result, a related boundedness result and the consistency of the discrete bilinear form, we can easily estimate the discretization error by the best approximation error with respect to the discrete norm. With the help of the approximation results from [11] and [10], we derive discretization error estimates taking into account that the exact solution can exhibit anisotropic regularity behavior, i.e., different regularity properties with respect to the time and to the space directions.

Finally, we have to solve one huge linear system $\mathbf{L}_h \mathbf{u}_h = \mathbf{f}_h$ of IgA equations defining all control points in space and time all at once. The fast generation and the fast solution of this

system is an issue. In our case, we can benefit from the special time-multipatch dG structure of the discretization that leads to a block-bidiagonal system matrix $\mathbf{L}_h = \text{blockbidiag}(-\mathbf{B}_i, \mathbf{A}_i)$, where the block-diagonal matrices \mathbf{A}_i , $i = 1, \dots, N$, and the block-subdiagonal matrices \mathbf{B}_i , $i = 2, \dots, N$, have tensor product representations. These properties lead to a fast generation of the matrix \mathbf{L}_h . The block-bidiagonal structure of the system matrix \mathbf{L}_h enables us to solve the system sequentially from one space-time patch to the next space-time patch similar to a time stepping scheme. However, we want to overcome this curse of sequentiality since we want to use the power of massively parallel computers with hundred or thousands of cores to solve this system efficiently. Similar to [19], we propose a space-time multigrid method that solves the complete system $\mathbf{L}_h \mathbf{u}_h = \mathbf{f}_h$ in parallel. In fact, we use the space-time multigrid method as preconditioner in a GMRES solver. The numerical results presented in the paper confirm not only our convergence rate estimates but also show the efficiency of the generation and solver technology proposed in the paper. The first numerical results for the lowest-order splines can be found in our proceedings paper [36] where we consider the simplified case of same smoothness of the solution in space and time.

The remainder of the paper is organized as follows. In Section 2, beside introducing some notations and preliminaries, the stable time-multipatch dG space-time IgA scheme is derived. Section 3 provides a complete a priori discretization error analysis, whereas Section 4 gives the matrix representation of our time-multipatch dG space-time IgA scheme and describes the parallel space-time multigrid solver. Finally, we present and discuss some first numerical results in Section 5, and draw some conclusions in Section 6.

2 The model problem and its stable space-time IgA scheme

2.1 Preliminaries

Let Ω be a bounded Lipschitz domain in \mathbb{R}^d , $d = 1, 2$, or 3 , with the boundary $\Gamma = \partial\Omega$. For any multi-index $\boldsymbol{\alpha} = (\alpha_1, \dots, \alpha_d)$ of non-negative integers $\alpha_1, \dots, \alpha_d$, we define the differential operator $\partial_x^{\boldsymbol{\alpha}} = \partial_{x_1}^{\alpha_1} \dots \partial_{x_d}^{\alpha_d}$, with $\partial_{x_j} = \partial/\partial x_j$, $j = 1, \dots, d$. For a non-negative integer ℓ , $C^\ell(\Omega)$ denotes the space of all continuous functions $v : \Omega \rightarrow \mathbb{R}$ whose partial derivatives $\partial_x^{\boldsymbol{\alpha}} v$ of all orders $|\boldsymbol{\alpha}| = \sum_{j=1}^d \alpha_j \leq \ell$ are continuous in Ω . As usual, $L_2(\Omega)$ denotes the Lebesgue space for which $\int_\Omega |v|^2 dx < \infty$, endowed with the norm $\|v\|_{L_2(\Omega)} = \left(\int_\Omega |v(x)|^2 dx \right)^{\frac{1}{2}}$, and $L^\infty(\Omega)$ denotes the functions that are essentially bounded. We define the standard Sobolev space

$$H^\ell(\Omega) = \{v \in L_2(\Omega) : \partial_x^{\boldsymbol{\alpha}} v \in L_2(\Omega) \text{ for all } |\boldsymbol{\alpha}| \leq \ell\},$$

endowed with the norm

$$\|v\|_{H^\ell(\Omega)} = \left(\sum_{0 \leq |\boldsymbol{\alpha}| \leq \ell} \|\partial_x^{\boldsymbol{\alpha}} v\|_{L_2(\Omega)}^2 \right)^{\frac{1}{2}},$$

whereas the trace space of $H^1(\Omega)$ is denoted by $H^{\frac{1}{2}}(\Gamma)$. Further, we introduce the subspace $H_0^1(\Omega) = \{v \in H^1(\Omega) : v = 0 \text{ on } \Gamma\}$ of all functions v from $H^1(\Omega)$ with zero traces on Γ . Let $J = (0, T)$ with some final time $T > 0$ be the time interval. For later use, we define the space-time cylinder $Q = \Omega \times J$ and its boundary parts $\Sigma = \partial\Omega \times J$, $\Sigma_T = \Omega \times \{T\}$ and $\Sigma_0 = \Omega \times \{0\}$ such that $\partial Q = \Sigma \cup \overline{\Sigma_0} \cup \overline{\Sigma_T}$, see an illustration in Fig. 1(a). Accordingly to the definition of $\partial_x^{\boldsymbol{\alpha}}$, we now define the spatial gradient $\nabla_x v = (\partial_{x_1} v, \dots, \partial_{x_d} v)$. Let ℓ and m be positive integers. For functions defined in the space-time cylinder Q , we define the Sobolev spaces

$$H^{\ell, m}(Q) = \{v \in L_2(Q) : \partial_x^{\boldsymbol{\alpha}} v \in L_2(Q) \text{ for } 0 \leq |\boldsymbol{\alpha}| \leq \ell, \text{ and } \partial_t^i v \in L_2(Q), i = 1, \dots, m\}, \quad (2.1)$$

and, in particular, the subspaces

$$H_0^{1,0}(Q) = \{v \in L_2(Q) : \nabla_x v \in [L_2(Q)]^d, v = 0 \text{ on } \Sigma\} \text{ and} \quad (2.2)$$

$$H_{0,0}^{1,1}(Q) = \{v \in L_2(Q) : \nabla_x v \in [L_2(Q)]^d, \partial_t v \in L_2(Q), v = 0 \text{ on } \Sigma, v = 0 \text{ on } \Sigma_T\}. \quad (2.3)$$

We equip the above spaces with the norms and seminorms

$$\|v\|_{H^{\ell,m}(Q)} = \left(\sum_{|\alpha| \leq \ell} \|\partial_x^{(\alpha_1, \dots, \alpha_d)} v\|_{L_2(Q)}^2 + \sum_{m_0=0}^m \|\partial_t^{m_0} v\|_{L_2(Q)}^2 \right)^{\frac{1}{2}} \text{ and} \quad (2.4a)$$

$$|v|_{H^{\ell,m}(Q)} = \left(\sum_{|\alpha|=\ell} \|\partial_x^{(\alpha_1, \dots, \alpha_d)} v\|_{L_2(Q)}^2 + \|\partial_t^m v\|_{L_2(Q)}^2 \right)^{\frac{1}{2}}. \quad (2.4b)$$

We recall Cauchy - Schwarz and Young's inequalities

$$\left| \int_{\Omega} uv \, dx \right| \leq \|u\|_{L_2(\Omega)} \|v\|_{L_2(\Omega)} \quad \text{and} \quad \left| \int_{\Omega} uv \, dx \right| \leq \frac{\epsilon}{2} \|u\|_{L_2(\Omega)}^2 + \frac{1}{2\epsilon} \|v\|_{L_2(\Omega)}^2 \quad (2.5)$$

that hold for all functions u and v from $L_2(\Omega)$ and for any fixed $\epsilon \in (0, \infty)$. We also recall Friedrichs' inequality that we later need in the form

$$\|v\|_{L_2(Q)} \leq C_{\Omega} \|\nabla_x v\|_{L_2(Q)}, \quad (2.6)$$

that holds for all $v \in H^1(Q)$ with vanishing trace on Σ , see proof of Friedrichs' inequality in [12].

In what follows, positive constants c and C appearing in inequalities are generic constants which do not depend on the mesh-size h . In many cases, we will indicate on what may the constants depend for an easier understanding of the proofs. Frequently, we will write $a \sim b$ meaning that $ca \leq b \leq Ca$ with generic positive constants c and C .

2.2 The model parabolic problem

Using the standard procedure and integration by parts with respect to both x and t , we can easily derive the following space-time variational formulation of (1.1): find $u \in H_0^{1,0}(Q)$ such that

$$a(u, v) = l(v) \quad \text{for all } v \in H_0^{1,1}(Q), \quad (2.7)$$

with the bilinear form

$$a(u, v) = - \int_Q u(x, t) \partial_t v(x, t) \, dx \, dt + \int_Q \nabla_x u(x, t) \cdot \nabla_x v(x, t) \, dx \, dt \quad (2.8)$$

and the linear form

$$l(v) = \int_Q f(x, t) v(x, t) \, dx \, dt + \int_{\Omega} u_0(x) v(x, 0) \, dx, \quad (2.9)$$

where the source $f \in L_2(Q)$ and the initial conditions $u_0 \in L_2(\Omega)$ are given.

For simplicity, we only consider homogeneous Dirichlet boundary conditions on Σ . However, the analysis presented in our paper can easily be generalized to other constellations of boundary conditions. The space-time variational formulation (2.7) has a unique solution, see, e.g. [31] and [32]. In these monographs, beside existence and uniqueness results, one can also find useful a priori estimates and regularity results.

Assumption 2.1 *We assume that the solution u of (2.7) belongs to $V = H_0^{1,0}(Q) \cap H^{\ell,m}(Q)$ with some $\ell \geq 2$ and $m \geq 1$.*

2.3 B-spline spaces and patch parametrizations

In this section, we briefly present the B-spline spaces and the form of the B-spline parametrizations for the physical space-time patches (subdomains). We refer to [13], [14] and [48] for a more detailed introduction to B-splines.

To describe more clearly the basic materials, we start with presenting the B-spline spaces for the univariate case. Let the integer p denotes the B-spline degree and the integer n_1 denotes the number of the basis functions. Consider, $\mathcal{Z} = \{0 = z_1, z_2, \dots, z_M = 1\}$ to be a partition of $[0, 1]$ with $[z_j, z_{j+1}]$, $j = 1, \dots, M - 1$ to be the intervals of the partition. Based on \mathcal{Z} , we consider a knot-vector $\Xi = \{0 = \xi_1 \leq \xi_2 \leq \dots \leq \xi_{n_1+p+1} = 1\}$ and the associated vector of the knot repetitions $\mathcal{M} = \{m_1, \dots, m_M\}$, this means,

$$\Xi = \left\{ \underbrace{0 = \xi_1, \dots, \xi_{m_1}}_{=z_1}, \underbrace{\xi_{m_1+1} = \dots = \xi_{m_1+m_2}}_{=z_2}, \dots, \underbrace{\xi_{n_1+p+1-m_M}, \dots, \xi_{n_1+p+1}}_{=z_M} = 1 \right\}. \quad (2.10)$$

We assume that $m_j \leq p$ for all internal knots. The B-spline basis functions are defined by the Cox-de Boor formula

$$B_{i,p} = \frac{x - \xi_i}{\xi_{i+p} - \xi_i} B_{i,p-1}(x) + \frac{\xi_{i+p+1} - x}{\xi_{i+p+1} - \xi_{i+1}} B_{i+1,p-1}(x) \quad (2.11)$$

where $B_{i,0}(x) = 1$ if $\xi_i \leq x \leq \xi_{i+1}$, and 0 otherwise.

The multivariate B-spline spaces can be derived through tensor product procedures of the univariate spaces. Let us consider the unit cube $\hat{Q} = (0, 1)^{d+1} \subset \mathbb{R}^{d+1}$, which we will refer to as the parametric domain. Following the same steps, let the integers p_k and n_k , which denote the given B-spline degree and the number of basis functions of the B-spline space in x_k -direction with $k = 1, \dots, d + 1$. We introduce the corresponding open-knot vectors $\Xi_n^k = \{0 = \xi_1^k \leq \xi_2^k \leq \dots \leq \xi_{n_k+p+1}^k = 1\}$, the vectors \mathcal{Z}_k and \mathcal{M}_k . We associate with each knot vector Ξ^k the B-spline basis functions $\hat{\mathbb{B}}_{\Xi^k, p_k}$ of degree p_k , for $k = 1, \dots, d + 1$. On the parametric domain \hat{Q} , we define the tensor-product B-spline space $\hat{\mathbb{B}}_{\Xi_n^{d+1}, p} = \otimes_{k=1}^{d+1} \hat{\mathbb{B}}_{\Xi_n^k, p}$, where $\Xi_n^{d+1} = (\Xi_n^1, \dots, \Xi_n^k, \dots, \Xi_n^{d+1})$.

The decomposition into space-time patches In practice, it is usually more convenient to describe the computational domain as a union of subdomains (patches) and to develop a multi-patch IgA approach. For our case, we will describe the space-time cylinder Q as a union of non-overlapping space-time patches Q_1, Q_2, \dots, Q_N . Consider a partition $0 = t_0 < t_1 < \dots < t_N = T$ of $[0, T]$ and let $J_n = (t_{n-1}, t_n)$. We define $Q_n = \Omega \times J_n$ and $\Sigma_n = \bar{Q}_{n+1} \cap \bar{Q}_n = \Omega \times \{t_n\}$ where we identify Σ_T and Σ_N . In that way, we have

$$\bar{Q} = \bigcup_{n=1}^N \bar{Q}_n, \quad \text{with} \quad \bar{Q}_{n+1} \cap \bar{Q}_n = \Sigma_n. \quad (2.12)$$

A schematic illustration for the general case $Q \subset \mathbb{R}^{d+1}$ is presented in Fig. 1(a), for the case of $Q \subset \mathbb{R}^2$ in Fig. 1(b), and for $Q \subset \mathbb{R}^3$ in Fig. 1(c). We proceed below by defining the approximation B-spline spaces in every Q_n as well the corresponding parametrizations.

Let us assume for simplicity that the B-spline degree is the same for all directions and for all the patches, i.e., $p_{n,k} = p$ for $k = 1, \dots, d + 1$, and let the integer n_k denote the the number of basis functions of the B-spline space in x_k -direction, respectively. For every $Q_n, n = 1, \dots, N$, we introduce the $(d + 1)$ -dimensional vector of knots $\Xi_n^{d+1} = (\Xi_n^1, \dots, \Xi_n^k, \dots, \Xi_n^{d+1})$, with the particular components given by $\Xi_n^k = \{0 = \xi_1^k \leq \xi_2^k \leq \dots \leq \xi_{n_k+p+1}^k = 1\}$. For all the internal knots, we assume that $m_j^k \leq p$, with m_j^k to be the associated multiplicities. The components Ξ_n^k of Ξ_n^{d+1} form a mesh $T_{h_n, \hat{Q}}^{(n)} = \{\hat{E}_m\}_{m=1}^{M_n}$ in \hat{Q} , where \hat{E}_m are the micro elements and h_n is the mesh size, which is defined as follows: given a micro element $\hat{E}_m \in T_{h_n, \hat{Q}}^{(n)}$, we set $\hat{h}_{\hat{E}_m} = \text{diam}(\hat{E}_m)$,

and we define $\hat{h}_n = \max\{\hat{h}_{\hat{E}_m}\}$. We set $\hat{h} = \max_{n=1,\dots,N}\{\hat{h}_n\}$. We refer the reader to [13] for more information about the meaning of the knot vectors in CAD and IgA.

Given the knot vector Ξ_n^k in every direction $k = 1, \dots, d+1$, we construct the associated univariate B-spline basis, $\mathbb{B}_{\Xi_n^k,p} = \{\hat{B}_{1,k}^{(n)}(\hat{x}_k), \dots, \hat{B}_{n_k,k}^{(n)}(\hat{x}_k)\}$ using the Cox-de Boor recursion formula (2.11), see, also [13] and [14] for more details. Accordingly, on the mesh $T_{h_n,\hat{Q}}^{(n)}$, the basis functions of the multivariate B-spline space $\hat{\mathbb{B}}_{\Xi_n^{d+1},p}$ are defined by the tensor-product of the corresponding univariate B-spline basis functions of $\mathbb{B}_{\Xi_n^k,p}$ spaces, that is

$$\hat{\mathbb{B}}_{\Xi_n^{d+1},p} = \otimes_{k=1}^{d+1} \mathbb{B}_{\Xi_n^k,p} = \text{span}\{\hat{B}_j^{(n)}(\hat{x})\}_{j=1}^{n_B=n_1 \cdots n_k \cdots n_{d+1}}, \quad (2.13)$$

where each $\hat{B}_j^{(n)}(\hat{x})$ has the form

$$\hat{B}_j^{(n)}(\hat{x}) = \hat{B}_{j_1}^{(n)}(\hat{x}_1) \cdots \hat{B}_{j_k}^{(n)}(\hat{x}_k) \cdots \hat{B}_{j_d}^{(n)}(\hat{x}_d), \text{ with } \hat{B}_{j_k}^{(n)}(\hat{x}_k) \in \hat{\mathbb{B}}_{\Xi_n^k,p}. \quad (2.14)$$

According to the IgA approach, every patch is described as a parametrization mapping by means of the a B-spline space defined in the in the parametric domain and the control grid. Precisely for our case, we assume that we are given the net of the control points $\mathbf{C}_j^{(n)}$ related to Q_n , and we parametrize each space-time patch Q_n by

$$\Phi_n : \hat{Q} \rightarrow Q_n, \quad x = \Phi_n(\hat{x}) = \sum_{j=1}^{n_B} \mathbf{C}_j^{(n)} \hat{B}_j^{(n)}(\hat{x}) \in Q_n, \quad (2.15)$$

where $\hat{x} = \Phi_n^{-1}(x)$, $n = 1, \dots, N$, cf. [13]. For every Q_n , $n = 1, \dots, N$, we construct a mesh $T_{h_{Q_n},Q_n}^{(n)} = \{E_m\}_{m=1}^{M_n}$, where the elements E_m are the images of $\hat{E}_m \in T_{h_n,\hat{Q}}^{(n)}$ under Φ_n , i.e., $E_m = \Phi_n(\hat{E}_m)$. Also, for each $E \in T_{h_i,\Omega_i}^{(i)}$, we denote its support extension by \tilde{E} , where the support extension is defined to be the interior of the set formed by the union of the supports of all B-spline functions whose supports intersects E . Accordingly to the parametric mesh, we denote $h_{E_m} = \text{diam}(E_m)$ and define $h_{Q_n} = \max\{h_{E_m} : E_m \in T_{h_{Q_n},Q_n}^{(n)}\}$, and the global physical mesh size is $h = \max h_{Q_n}$. For $n = 1, \dots, N$, we construct the B-spline space $\mathbb{B}_{\Xi_n^{d+1},p}$ on Q_n by

$$\mathbb{B}_{\Xi_n^{d+1},p} := \text{span}\{B_j^{(n)}|_{Q_n} : B_j^{(n)}(x) = \hat{B}_j^{(n)} \circ \Phi_n^{-1}(x), \text{ for } j = 1, \dots, n_B\}. \quad (2.16)$$

The global B-spline space V_h with components on every $\mathbb{B}_{\Xi_i^d,p}$ is defined by

$$V_h := V_{h_1}^{(1)} \times \dots \times V_{h_N}^{(N)} := \mathbb{B}_{\Xi_1^{d+1},p} \times \dots \times \mathbb{B}_{\Xi_N^{d+1},p}. \quad (2.17)$$

Assumption 2.2 *The meshes $T_{h_n,\hat{Q}}^{(n)}$ are uniform, i.e., for every $\hat{E} \in T_{h_n,\hat{Q}}^{(n)}$ there exist a number $\gamma_n > 0$ such that $\gamma_n \leq \hat{h}_n/\rho_{\hat{E}}$, where $\rho_{\hat{E}}$ is the radius of the inscribed circle of \hat{E} .*

Remark 2.1. Since the parametrizations Φ_n , $n = 1, \dots, N$, are fixed, under the Assumption 2.2, we have that $\hat{h}_n \sim h_{Q_n}$. Thus, below, we will use h_n , for denoting any of the mesh sizes, parametric or physical. For simplicity, we assume that $h_n \leq 1$ for all $n = 1, \dots, N$.

The parametrization mappings Φ_n , $n = 1, \dots, N$ can be considered to be bi-Lipschitz homeomorphisms, [10]. For simplifying the analysis, we further consider the following regularity properties on Φ_n , $n = 1, \dots, N$.

Assumption 2.3 *Assume that every Φ_n and Φ_n^{-1} , $n = 1, \dots, N$, are sufficiently smooth, (C^1 diffeomorphisms), and there exist constants $0 < c < C$ such that $c \leq |\det J_{\Phi_n}| \leq C$, where J_{Φ_n} is the Jacobian matrix of Φ_n , i.e., $J_{\Phi_n} = \frac{\partial(\Phi_{n,1}, \dots, \Phi_{n,d+1})}{\partial(\hat{x}_1, \dots, \hat{t})}$.*

Assumption 2.3 helps on simplifying the form of the constants, which appear in the relations between the norms of the pull-back solution and the physical relevant solution.

Corollary 2.1. *Let the Assumption 2.3 and let $u \in H^{\ell,m}(Q)$ with $\ell \geq 2$ and $m \geq 1$. Then its pull-back $\hat{u} = u \circ \Phi_n \in H^{1,1}(\hat{Q})$ and there exist constants c_1 and c_2 depending only on Φ_n and Φ_n^{-1} and not on u , such that $c_1 \|\hat{u}\|_{H^{1,1}(\hat{Q})} \leq \|u\|_{H^{1,1}(Q_n)} \leq c_2 \|\hat{u}\|_{H^{1,1}(\hat{Q})}$.*

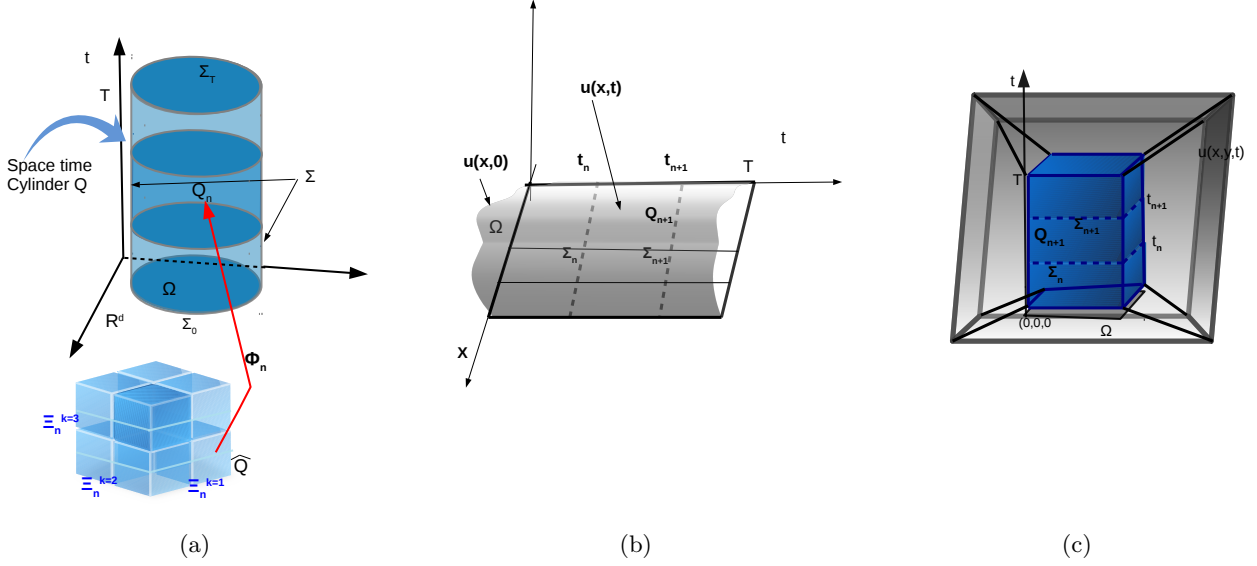


Fig. 1. (a) The decomposition of the space type cylinder Q into space-time patches Q_n , together with the mesh in the parametric domain \hat{Q} produced by the knot-vectors Ξ_n^k , (b) The space-time patches Q_n with their interfaces and the graph of $u(x, t)$ for the case of $Q \subset \mathbb{R}^2$, (c) The space-time patches Q_n with their interfaces and the graph of $u(x, t)$ for the case of $Q \subset \mathbb{R}^3$.

To keep the notation simple, in what follows, we will use the notation $\mathcal{T}_N(Q) := \{Q_1, Q_2, \dots, Q_N\}$ for the decomposition (2.12) and the sup-index n to denote the restrictions to Q_n , e.g., $u^n := u|_{Q_n}$. We denote the global discontinuous B-spline space and the local continuous patch-wise B-spline spaces by

$$V_{0h} = \{v_h \in L_2(Q) : v_h|_{Q_n} \in \mathbb{B}_{\Xi_i^{d+1}, p}(Q_n), \text{ for } n = 1, \dots, N, \text{ and } v_h|_{\Sigma} = 0\}, \quad (2.18a)$$

$$V_{0h}^{(n)} = \{v_h \in \mathbb{B}_{\Xi_i^{d+1}, p}(Q_n), \text{ for } n = 1, \dots, N, \text{ and } v_h|_{\Sigma} = 0\}. \quad (2.18b)$$

Notice that $v_h \in V_{0h}$ is discontinuous across Σ_n . We introduce the notation

$$v_{h,+}^n = \lim_{\varepsilon \rightarrow 0^+} v_h(t_n + \varepsilon), \quad v_{h,-}^n = \lim_{\varepsilon \rightarrow 0^-} v_h(t_n + \varepsilon), \quad \llbracket v_h \rrbracket^n = v_{h,+}^n - v_{h,-}^n, \quad \llbracket v_h \rrbracket^0 = v_{h,+}^0, \quad (2.19)$$

where $\llbracket v_h \rrbracket^n$ denotes the jump of v_h across Σ_n for $n \geq 1$, and $\llbracket v_h \rrbracket^0 = v_{h,+}^0$ denotes the jump across Σ_0 . Decomposition (2.12) helps us to consider N local problems posed on each space-time patch Q_n . In view of (2.19), for a smooth function u we have that $\llbracket u \rrbracket^n = u_+^n - u_-^n = 0$ for $n \geq 1$, and accordingly define $\llbracket u \rrbracket^0 = u|_{\Sigma_0}$.

2.4 Stable multipatch space-time dG IgA discretization

Let us consider the space-time patch Q_n , with the outer normal to ∂Q to be $\mathbf{n} = (n_1, \dots, n_d, n_{d+1}) = (\mathbf{n}_x, n_t)$. For the being time, we assume that u^{n-1} is known. Let $v_h^n \in V_{0h}^{(n)}$ and $w_h^n = v_h^n + \theta_n h_n \partial_t v_h^n$ with some positive parameter θ_n , that will be defined later. Note that $w_h^n|_{\Sigma} = 0$. Multiplying

$\partial_t u - \Delta u = f$ by w_h^n , integrating over Q_n , and applying integration by parts, we arrive at the variational identity

$$\begin{aligned} a_{Q_n}(u, v_h^n) &= \int_{Q_n} \partial_t u (v_h^n + \theta_n h_n \partial_t v_h^n) + \nabla_x u \cdot \nabla_x v_h^n + \theta_n h_n \nabla_x u \cdot \nabla_x \partial_t v_h^n \, dx \, dt \\ &\quad - \int_{\partial Q_n} n_x \cdot \nabla_x u (v_h^n + \theta_n h_n \partial_t v_h^n) \, ds + \int_{\Sigma_{n-1}} u_+^{n-1} v_{h,+}^{n-1} \, ds \\ &= \int_{Q_n} f (v_h^n + \theta_n h_n \partial_t v_h^n) \, dx \, dt + \int_{\Sigma_{n-1}} u_-^{n-1} v_{h,+}^{n-1} \, ds, \quad \text{for } 1 \leq n \leq N, \end{aligned} \quad (2.20)$$

where we used that $u_-^{n-1} = u_+^{n-1} = u^{n-1}$ on every Σ_n . Furthermore, using that $n_x|_{\Sigma_n} = 0$, and $w_h = 0$ on Σ , we have

$$\begin{aligned} a_{Q_n}(u, v_h^n) &= \int_{Q_n} \partial_t u (v_h^n + \theta_n h_n \partial_t v_h^n) + \nabla_x u \cdot \nabla_x v_h^n + \theta_n h_n \nabla_x u \cdot \nabla_x \partial_t v_h^n \, dx \, dt \\ &\quad + \int_{\Sigma_{n-1}} \llbracket u \rrbracket^{n-1} v_{h,+}^{n-1} \, ds = \int_{Q_n} f (v_h^n + \theta_n h_n \partial_t v_h^n) \, dx \, dt, \end{aligned} \quad (2.21a)$$

for all $n = 1, \dots, N$. Summing over all Q_n , we conclude that

$$a(u, v_h) = \sum_{n=1}^N a_{Q_n}(u, v_h^n) = \sum_{n=1}^N \int_{Q_n} f (v_h^n + \theta_n h_n \partial_t v_h^n) \, dx \, dt, \quad (2.21b)$$

where above the $a(\cdot, \cdot)$ is considered to be the global bilinear form. Now, the space-time dG IgA variational scheme for (1.1) can be formulated as follows: Find $u_h \in V_{0h}$ such that

$$a_h(u_h, v_h) = l_h(v_h), \quad \forall v_h \in V_{0h}, \quad (2.22a)$$

where

$$\begin{aligned} a_h(u_h, v_h) &= \sum_{n=1}^N a_{Q_n}(u_h, w_h^n) \\ &= \sum_{n=1}^N \int_{Q_n} \partial_t u_h^n (v_h^n + \theta_n h_n \partial_t v_h^n) + \nabla_x u_h^n \cdot \nabla_x v_h^n + \theta_n h_n \nabla_x u_h^n \cdot \nabla_x \partial_t v_h^n \, dx \, dt \\ &\quad + \sum_{n=2}^N \int_{\Sigma_{n-1}} \llbracket u_h \rrbracket^{n-1} v_{h,+}^{n-1} \, ds + \int_{\Sigma_0} \llbracket u_h \rrbracket^0 v_{h,+}^0 \, ds, \\ l_h(v_h) &= \sum_{n=1}^N \int_{Q_n} f (v_h^n + \theta_n h_n \partial_t v_h^n) \, dx \, dt + \int_{\Sigma_0} u_0 v_{h,+}^0 \, ds, \end{aligned} \quad (2.22b)$$

where $\llbracket \cdot \rrbracket$ is as in (2.19). Below for simplifying the jump expressions, we use the consolidated expression $\sum_{n=1}^N \int_{\Sigma_{n-1}} \llbracket u_h \rrbracket^{n-1} v_{h,+}^{n-1} \, ds$.

The classical properties for the discrete bilinear form. We cite a few auxiliary results that will be used in the error analysis below. For the proofs, we refer to [7], [15], [9], see also discussion in [37].

Lemma 2.1. *Let the patch $Q_n \in \mathcal{T}_N(Q)$, and let $v \in H^1(Q_n)$, $v_h \in \mathbb{B}_{\Xi_n^{d+1,p}}$ and $E \in T_{h_n, Q_n}^{(n)}$. Then there are positive constants C_{tr} , $C_{inv,0}$ and $C_{inv,1}$ depending on Φ_n and the quasi-uniform properties of $T_{h_n, Q_n}^{(n)}$, such that*

$$\|v\|_{L_2(\partial E)}^2 \leq C_{tr} h_n^{-1} (\|v\|_{L_2(E)} + h_n |v|_{H^1(E)})^2, \quad (2.23a)$$

$$\|v_h\|_{L_2(\partial E)}^2 \leq C_{inv,0} h_n^{-1} \|v_h\|_{L_2(E)}^2, \quad (2.23b)$$

$$\|\nabla v_h\|_{L_2(E)}^2 \leq C_{inv,1} h_n^{-2} \|v_h\|_{L_2(E)}^2. \quad (2.23c)$$

By the inequalities (2.23), we can easily infer that

$$\|\partial_t v_h\|_{L_2(\partial E)}^2 \leq C_{inv,1} h_n^{-2} \|v_h\|_{L_2(E)}^2, \quad \text{and} \quad \|\partial_t \partial_{x_i} v_h\|_{L_2(\partial E)}^2 \leq C_{inv,1} h_n^{-2} \|\partial_{x_i} v_h\|_{L_2(E)}^2. \quad (2.24)$$

Motivated by (2.22b), we define the norm on V_{0h}

$$\|v\|_{dG} = \left(\sum_{n=1}^N \left(\|\nabla_x v\|_{L_2(Q_n)}^2 + \theta_n h_n \|\partial_t v\|_{L_2(Q_n)}^2 + \frac{1}{2} \|[[v]]^{n-1}\|_{L_2(\Sigma_{n-1})}^2 \right) + \frac{1}{2} \|v\|_{L_2(\Sigma_N)}^2 \right)^{\frac{1}{2}}. \quad (2.25)$$

Lemma 2.2. *The discrete bilinear form $a_h(\cdot, \cdot)$ defined in (2.22b) is V_{0h} -elliptic, i.e., holds*

$$a_h(v_h, v_h) \geq C_e \|v_h\|_{dG}^2, \quad \text{for } v_h \in V_{0h}, \quad (2.26)$$

where $C_e = \frac{1}{2}$ for $\theta_n \leq C_{inv,0}^{-2}$.

Proof. Using Green's formula $\int_{Q_n} \partial_t v_h v_h + v_h \partial_t v_h dx dt = \int_{\partial Q_n} n_t v_h^2 ds$, we obtain the identity

$$\int_{Q_n} \partial_t v_h v_h = \frac{1}{2} \int_{Q_n} \partial_t v_h^2 dx dt = \frac{1}{2} \int_{\Sigma_n} (v_{h,-})^2 ds - \frac{1}{2} \int_{\Sigma_{n-1}} (v_{h,+})^2 ds. \quad (2.27)$$

The definition of a_{Q_n} and identity (2.27) yield

$$\begin{aligned} a_{Q_n}(v_h, v_h) &= \int_{Q_n} \frac{1}{2} \partial_t v_h^2 + \theta_n h_n (\partial_t v_h)^2 + |\nabla_x v_h|^2 + \frac{\theta_n h_n}{2} \partial_t |\nabla_x v_h|^2 dx dt + \int_{\Sigma_{n-1}} [[v_h]]^{n-1} v_{h,+}^{n-1} ds \\ &= \int_{Q_n} \theta_n h_n (\partial_t v_h)^2 + |\nabla_x v_h|^2 dx dt + \int_{\partial Q_n} \frac{\theta_n h_n}{2} |\nabla_x v_h|^2 n_t \\ &\quad + \int_{\Sigma_{n-1}} \left((v_{h,+}^{n-1})^2 - v_{h,-}^{n-1} v_{h,+}^{n-1} - \frac{1}{2} (v_{h,+}^{n-1})^2 \right) ds + \frac{1}{2} \int_{\Sigma_n} (v_{h,-}^n)^2 ds \\ &= \theta_n h_n \|\partial_t v_h\|_{L_2(Q_n)}^2 + \|\nabla_x v_h\|_{L_2(Q_n)}^2 + \frac{\theta_n h_n}{2} \left(\|\nabla_x v_h\|_{L_2(\Sigma_n)}^2 - \|\nabla_x v_h\|_{L_2(\Sigma_{n-1})}^2 \right) \\ &\quad + \int_{\Sigma_{n-1}} \left((v_{h,+}^{n-1})^2 - v_{h,-}^{n-1} v_{h,+}^{n-1} - \frac{1}{2} (v_{h,+}^{n-1})^2 \right) ds + \frac{1}{2} \int_{\Sigma_n} (v_{h,-}^n)^2 ds \\ &\geq \theta_n h_n \|\partial_t v_h\|_{L_2(Q_n)}^2 + \|\nabla_x v_h\|_{L_2(Q_n)}^2 - \frac{\theta_n h_n}{2} \|\nabla_x v_h\|_{L_2(\Sigma_{n-1})}^2 \\ &\quad + \int_{\Sigma_{n-1}} \left(\frac{1}{2} (v_{h,+}^{n-1})^2 - v_{h,-}^{n-1} v_{h,+}^{n-1} \right) ds + \frac{1}{2} \int_{\Sigma_n} (v_{h,-}^n)^2 ds \\ &\geq \theta_n h_n \|\partial_t v_h\|_{L_2(Q_n)}^2 + \left(1 - \frac{\theta_n C_{inv,0}^2}{2} \right) \|\nabla_x v_h\|_{L_2(Q_n)}^2 \\ &\quad + \int_{\Sigma_{n-1}} \left(\frac{1}{2} (v_{h,+}^{n-1})^2 - v_{h,-}^{n-1} v_{h,+}^{n-1} \right) ds + \frac{1}{2} \int_{\Sigma_n} (v_{h,-}^n)^2 ds, \end{aligned} \quad (2.28)$$

where we have used (2.23) at the last step in (2.28). Summing over all Q_n , and using (2.19), we obtain

$$\begin{aligned} a_h(v_h, v_h) &= \sum_{n=1}^N a_{Q_n}(v_h, v_h) \geq \sum_{n=1}^N \theta_n h_n \|\partial_t v_h\|_{L_2(Q_n)}^2 + \left(1 - \frac{\theta_n C_{inv,0}^2}{2} \right) \|\nabla_x v_h\|_{L_2(Q_n)}^2 \\ &\quad + \sum_{n=1}^N \frac{1}{2} \|[[v_h]]^{n-1}\|_{L_2(\Sigma_{n-1})}^2 + \frac{1}{2} \|v_{h,-}^N\|_{L_2(\Sigma_N)}^2. \end{aligned}$$

Choosing $0 < \theta_n \leq C_{inv,0}^{-2}$ the result follows easily by setting $C_e = \frac{1}{2}$. ■

Remark 2.2 (a-priori bound). Using the discrete solution u_h as test function in (2.22a), the inequalities defined in (2.5) and (2.6) yield

$$\begin{aligned}
C_e \|u_h\|_{dG}^2 &\leq a_h(u_h, u_h) \leq |l_h(u_h)| \leq \left| \sum_{n=1}^N \int_{Q_n} f(u_h^n + \theta_n h_n \partial_t u_h^n) dx dt \right| + \left| \int_{\Sigma_0} u_0 u_{h,+}^0 ds \right| \\
&\leq \|f\|_{L_2(Q)} \left(\sum_{n=1}^N \|u_h^n\|_{L_2(Q_n)}^2 \right)^{\frac{1}{2}} + \sum_{n=1}^N (\theta_n h_n)^{\frac{1}{2}} \|f\|_{L_2(Q_n)} (\theta_n h_n)^{\frac{1}{2}} \|\partial_t u_h^n\|_{L_2(Q_n)} + \|u_0\|_{L_2(\Sigma_0)} \|u_{h,+}^0\|_{L_2(\Sigma_0)} \\
&\leq \|f\|_{L_2(Q)} \left(\sum_{n=1}^N C_\Omega \|\nabla_x u_h^n\|_{L_2(Q_n)}^2 \right)^{\frac{1}{2}} + \theta_{max} h \|f\|_{L_2(Q)} \left(\sum_{n=1}^N \theta_n h_n \|\partial_t u_h^n\|_{L_2(Q_n)}^2 \right)^{\frac{1}{2}} + \sqrt{2} \|u_0\|_{L_2(\Sigma_0)} \|u_h\|_{dG} \\
&\leq \sqrt{2} c_{stab} \left(\|f\|_{L_2(Q)} + \|u_0\|_{L_2(\Sigma_0)} \right) \|u_h\|_{dG},
\end{aligned} \tag{2.29}$$

where $h = \max_n \{h_n\}$, and c_{stab} depends on the constants in (2.6) and on $\theta_{max} = \max_n \{\theta_n\}$. By (2.29), we can immediately get the a-priori bound $\|u_h\|_{dG} \leq C(\|f\|_{L_2(Q)} + \|u_0\|_{L_2(\Sigma_0)})$.

Later, in the discretization error analysis, we need continuity properties for $a_h(\cdot, \cdot)$. Let V and V_{0h} are the spaces defined in Assumption 2.1 and in (2.18). We define the space $V_{0h,*} = V + V_{0h}$ endowed with the norm

$$\|v\|_{dG,*} = \left(\|v\|_{dG}^2 + \sum_{n=1}^N (\theta_n h_n)^{-1} \|v\|_{L_2(Q_n)}^2 + \sum_{n=2}^N \|v_-^{n-1}\|_{L_2(\Sigma_{n-1})}^2 \right)^{\frac{1}{2}}. \tag{2.30}$$

Lemma 2.3. *Let $u \in V_{0h,*}$. Then for $v_h \in V_{0h}$ holds*

$$a_h(u, v_h) \leq c_b \|u\|_{dG,*} \|v_h\|_{dG}, \tag{2.31}$$

where $c_b = \max(C_{inv,1} \theta_{max}, 2)$ with $\theta_{max} = \max_n \{\theta_n\} \leq C_{inv,0}^{-2}$.

Proof. We recall (2.19) and $\llbracket u \rrbracket^0 = u|_{\Sigma_0}$. For the first and the interface jump terms of a_h , we use (2.27) and (2.5) and obtain

$$\begin{aligned}
&\sum_{n=1}^N \left(\int_{Q_n} \partial_t u v_h dx dt + \int_{\Sigma_{n-1}} \llbracket u \rrbracket^{n-1} v_{h,+}^{n-1} ds \right) \\
&= - \sum_{n=1}^N \int_{Q_n} u \partial_t v_h dx dt + \sum_{n=1}^N \left(\int_{\Sigma_n} u v_h ds - \int_{\Sigma_{n-1}} u v_h ds + \int_{\Sigma_{n-1}} \llbracket u \rrbracket^{n-1} v_{h,+}^{n-1} ds \right) \\
&\leq \left(\sum_{n=1}^N (\theta_n h_n)^{-1} \left(\int_{Q_n} u^2 dx dt \right)^2 \right)^{\frac{1}{2}} \left(\sum_{n=1}^N \theta_n h_n \left(\int_{Q_n} \partial_t v_h^2 dx dt \right)^2 \right)^{\frac{1}{2}} \\
&+ \sum_{n=2}^N \int_{\Sigma_{n-1}} (v_{h,-}^{n-1} - v_{h,+}^{n-1}) u_-^{n-1} ds + \int_{\Sigma_N} v_{h,-}^N u_-^N ds \\
&\leq \left(\sum_{n=1}^N (\theta_n h_n)^{-1} \left(\int_{Q_n} u^2 dx dt \right)^2 \right)^{\frac{1}{2}} \left(\sum_{n=1}^N \theta_n h_n \left(\int_{Q_n} \partial_t v_h^2 dx dt \right)^2 \right)^{\frac{1}{2}} \\
&+ \left(\sum_{n=2}^N \|v_{h,-}^{n-1} - v_{h,+}^{n-1}\|_{L_2(\Sigma_{n-1})}^2 \right)^{\frac{1}{2}} \left(\sum_{n=2}^N \|u_-^{n-1}\|_{L_2(\Sigma_{n-1})}^2 \right)^{\frac{1}{2}} + \|u_-^N\|_{L_2(\Sigma_N)} \|v_{h,-}^N\|_{L_2(\Sigma_N)} \\
&\leq \left(\sum_{n=1}^N (\theta_n h_n)^{-1} \left(\int_{Q_n} u^2 dx dt \right)^2 \right)^{\frac{1}{2}} \left(\sum_{n=1}^N \theta_n h_n \left(\int_{Q_n} \partial_t v_h^2 dx dt \right)^2 \right)^{\frac{1}{2}} \\
&+ \sqrt{2} \left(\frac{1}{2} \sum_{n=1}^N \|\llbracket v_h \rrbracket^{n-1}\|_{L_2(\Sigma_{n-1})}^2 + \frac{1}{2} \|v_h^N\|_{L_2(\Sigma_N)}^2 \right)^{\frac{1}{2}} \sqrt{2} \left(\sum_{n=2}^N \|u_-^{n-1}\|_{L_2(\Sigma_{n-1})}^2 + \frac{1}{2} \|u_-^N\|_{L_2(\Sigma_N)}^2 \right)^{\frac{1}{2}}.
\end{aligned} \tag{2.32}$$

For the second term, an application of Cauchy-Schwartz yields

$$\begin{aligned} & \sum_{n=1}^N \int_{Q_n} (\theta_n h_n)^{\frac{1}{2}} \partial_t u (\theta_n h_n)^{\frac{1}{2}} \partial_t v_h \, dx \, dt + \sum_{n=1}^N \int_{Q_n} \nabla_x u \cdot \nabla_x v_h \, dx \, dt \\ & \leq \left(\sum_{n=1}^N \theta_n h_n \|\partial_t u\|_{L_2(Q_n)}^2 \right)^{\frac{1}{2}} \left(\sum_{n=1}^N \theta_n h_n \|\partial_t v_h\|_{L_2(Q_n)}^2 \right)^{\frac{1}{2}} + \left(\sum_{n=1}^N \|\nabla_x u\|_{L_2(Q_n)}^2 \right)^{\frac{1}{2}} \left(\sum_{n=1}^N \|\nabla_x v_h\|_{L_2(Q_n)}^2 \right)^{\frac{1}{2}}. \end{aligned} \quad (2.33)$$

For the last term, we apply Cauchy-Schwartz and inverse inequalities to show

$$\begin{aligned} & \sum_{n=1}^N \int_{Q_n} \nabla_x u \cdot (\theta_n h_n) \nabla_x \partial_t v_h \, dx \, dt \leq \left(\sum_{n=1}^N \|\nabla_x u\|_{L_2(Q_n)}^2 \right)^{\frac{1}{2}} \left(\sum_{n=1}^N (\theta_n h_n)^2 \sum_{i=1}^d \int_{Q_n} (\partial_t \partial_{x_i} v_h)^2 \, dx \, dt \right)^{\frac{1}{2}} \\ & \leq \left(\sum_{n=1}^N \|\nabla_x u\|_{L_2(Q_n)}^2 \right)^{\frac{1}{2}} \left(\sum_{n=1}^N (\theta_n h_n)^2 C_{inv,1} h_n^{-2} \sum_{i=1}^d \int_{Q_n} (\partial_{x_i} v_h)^2 \, dx \, dt \right)^{\frac{1}{2}} \\ & \leq C_{inv,1} \theta_{max} \left(\sum_{n=1}^N \|\nabla_x u\|_{L_2(Q_n)}^2 \right)^{\frac{1}{2}} \left(\sum_{n=1}^N \|\nabla_x v_h\|_{L_2(Q_n)} \right)^{\frac{1}{2}}, \end{aligned} \quad (2.34)$$

where $\theta_{max} = \max_n \{\theta_n\} \leq C_{inv,0}^{-2}$. Gathering together the bounds (2.32), (2.33) and (2.34) and setting $c_b = \max(C_{inv,1} \theta_{max}, 2)$ yields the desired result. \blacksquare

Lemma 2.4. *Let Assumption 2.1 and let $u_h \in V_{0h}$ be the dG IgA solution of (2.22a). Then*

$$a_h(u - u_h, v_h) = 0, \quad \text{for } v_h \in V_{0h}. \quad (2.35)$$

Proof. Let $v_h \in V_{0h}$. Since $u \in V$ and $w_h = (v_h + \theta_n h_n \partial_t v_h)|_{\Sigma} = 0$ then $\int_{\Sigma_{n-1}} \llbracket u^n \rrbracket v_h \, ds = 0$, for $2 \leq n \leq N$. Moreover, u satisfies (2.21b). Comparing (2.21) and (2.22), we can infer (2.35). \blacksquare

3 A priori discretization error analysis

Based on the quasi-interpolation estimates presented in [7],[10], see also [48] and [37], we construct below quasi-interpolants $\Pi_h^{(n)} : H^{\ell,m}(Q_n) \rightarrow \mathbb{B}_{\Xi_i^{d+1},p}(Q_n)$, for $n = 1, \dots, N$, suitable for providing anisotropic interpolation estimates. Utilizing these estimates, we show the desirable anisotropic error estimates at the end of this section.

3.1 Multivariate quasi interpolants in \widehat{Q}

Let $\mathcal{Z} = \{0 = z_1, z_2, \dots, z_M = 1\}$ be a partition of $I = (0, 1)$ with $I_j = (z_j, z_{j+1})$, $j = 1, \dots, M-1$ to be the intervals of the partition and with mesh size $h = \max_j \{|I_j|\}$. Based on \mathcal{Z} , we consider a knot-vector $\Xi = \{0 = \xi_1 \leq \xi_2 \leq \dots \leq \xi_{n+p+1} = 1\}$ and the associated vector of the knot multiplicities $\mathcal{M} = \{m_1, \dots, m_M\}$. Let the integers s, ℓ be such that $0 \leq s \leq \ell \leq p+1$ and let $f \in H^\ell(I)$. Based on the quasi-interpolation estimates presented in [48], [10], we can construct a quasi-interpolant $\widehat{\Pi}_h : H^\ell(I) \rightarrow \widehat{\mathbb{B}}_{\Xi,p}(I)$, such that the following interpolation estimate holds true

$$|f - \widehat{\Pi}_h f|_{H^s(I)} \leq C h^{\ell-s} \|f\|_{H^\ell(I)}, \quad (3.1)$$

where the constant $C > 0$ depends on p and uniformity parameters of the partition. The previous construction of the univariate quasi-interpolation can be extended to the multi-dimensional case by applying tensor-product construction procedures as those presented in Section 2.3. For example, let $f \in H^\ell(\widehat{Q})$ with $\ell \geq 1$, and for $k = 1, \dots, d+1$, let $\widehat{\Pi}_{\Xi_h^k}$ be the corresponding k -th

univariate quasi-interpolant onto $\widehat{\mathbb{B}}_{\Xi_n^k}$. We construct the multi-dimensional B-spline interpolant $\widehat{\Pi}_{\Xi_n^{d+1}}$ as

$$\widehat{\Pi}_{\Xi_n^{d+1}} f = \otimes_{k=1}^{d+1} \widehat{\Pi}_{\Xi_n^k} f. \quad (3.2)$$

The general quasi-interpolation properties of the produced multivariate B-spline interpolants are inherited by the corresponding properties of the univariate interpolants. We refer to [48], [7] and [10], for a comprehensive analysis for constructing tensor-product B-spline interpolants.

3.2 Anisotropic quasi-interpolation in space-time patches Q_n

Let $f \in H^{\ell,m}(Q)$, with $\ell \geq 2$ and $m \geq 1$, and as usual we denote by $f_n = f|_{Q_n}$, for $n = 1, \dots, N$ its restriction on the space-time patches. Further, we denote by $\hat{f}_n = f \circ \Phi_n$ its pull-back function. We note that \hat{f}_n in general does not inherit the regularity of f but rather belongs to a bent-Sobolev space

$$\mathcal{H}^\ell(\widehat{Q}) = \mathcal{H}^{\ell_1}(I) \otimes \dots \otimes \mathcal{H}^{\ell_d}(I) \otimes \mathcal{H}^{\ell_{d+1}}(I), \quad (3.3)$$

that allows less regularity across the microelement interfaces, where in (3.3), $\mathcal{H}^{\ell_i}(I)$, $i = 1, \dots, d+1$ are the corresponding univariate bent-Sobolev spaces, [7, 10]. For showing the anisotropic quasi-interpolation estimates of interest, we have been strongly inspired by the results presented in [11] and in [10], which are suitable for anisotropic meshes. The generalization here is that we give anisotropic interpolation estimates that follow the anisotropic regularity of the solution. In the spirit of (3.2), we define in \widehat{Q} , the interpolant $\widehat{\Pi}_{\Xi_n^{d+1}} \hat{f}_n$ of the pull-back \hat{f}_n . For simplicity, we shall write $\widehat{\Pi}_h^{(n)}$ instead of $\widehat{\Pi}_{\Xi_n^{d+1}}$. Accordingly, we define in the space-time patches \widehat{Q}_n the quasi-interpolant of f_n as $\Pi_h^{(n)} f_n = (\widehat{\Pi}_h^{(n)} \hat{f}_n) \circ \Phi_n^{-1}$. By extension, we can define the global interpolant $\Pi_h : H^{\ell,m}(Q) \rightarrow V_h$ as, $(\Pi_h f)|_{Q_n} = \Pi_h^{(n)} f_n$, see e.g., [10]. Before giving estimates on how well $\widehat{\Pi}_h^{(n)} f$ approximates $f \in H^{\ell,m}(Q)$, some terminology is required.

We recall by Section 2.1 the definition of the differential operator $D^{(\alpha,m)}$, that is,

$$D^{(\alpha,m)} f := D^{(\alpha_1, \dots, \alpha_d, m)} f = \frac{\partial^{\alpha_1} \dots \partial^{\alpha_d} \partial^m}{\partial x_1^{\alpha_1} \dots \partial x_d^{\alpha_d} \partial t^m} f. \quad (3.4)$$

In order to derive the anisotropic estimate, we need to introduce the derivatives with respect to the coordinate system that is naturally introduced by the mappings $\Phi_n : \widehat{Q} \rightarrow Q_n$, see (2.15). We note again that, the mappings Φ_n are constructed on relatively coarse meshes and are highly smooth (polynomials) on the microelements of those meshes.

We recall that the columns of the Jacobian matrix of Φ_n , see (2.15) and Assumption 2.3, have the form

$$\left[\frac{\partial \Phi_{n,1}}{\partial \hat{x}_i}, \dots, \frac{\partial \Phi_{n,d}}{\partial \hat{x}_i}, \frac{\partial \Phi_{n,d+1}}{\partial \hat{x}_i} \right]^\top = \left[\frac{\partial \Phi_{n,1}}{\partial \hat{x}_i}, \dots, \frac{\partial \Phi_{n,d}}{\partial \hat{x}_i}, 0 \right]^\top, \quad (3.5)$$

where we have used above that $\frac{\partial \Phi_{n,d+1}}{\partial \hat{x}_i} = 0$ for $i = 1, \dots, d$, which easily follows by the tensor-product constructing properties of each Φ_n . Denote $\mathbf{g}_{n,i}(x, t) = \left[\frac{\partial \Phi_{n,1}}{\partial \hat{x}_i}(\Phi_n^{-1}(x, t)), \dots, \frac{\partial \Phi_{n,d}}{\partial \hat{x}_i}(\Phi_n^{-1}(x, t)), 0 \right]$. We introduce the derivatives of f with respect to the spatial Φ_n coordinates. The first derivatives are just the directional derivatives with respect to $\mathbf{g}_{n,i}$ for $i = 1, \dots, d$, i.e.,

$$\begin{aligned} \frac{\partial f(x, t)}{\partial \mathbf{g}_{n,1}} &= \nabla f(x, t) \cdot \mathbf{g}_{n,1}(x, t), \\ &\vdots \\ \frac{\partial f(x, t)}{\partial \mathbf{g}_{n,d}} &= \nabla f(x, t) \cdot \mathbf{g}_{n,d}(x, t). \end{aligned} \quad (3.6a)$$

The ‘‘one-directional’’ high-order derivatives are defined accordingly as

$$\frac{\partial^{\alpha_i} f}{\partial \mathbf{g}_{n,i}^{\alpha_i}} = \frac{\partial}{\underbrace{\partial \mathbf{g}_{n,i}}_{\alpha_i\text{-times}}} \left(\dots \left(\frac{\partial f}{\partial \mathbf{g}_{n,i}} \right) \right). \quad (3.6b)$$

Let the multi-index $\boldsymbol{\alpha} = (\alpha_1, \dots, \alpha_d)$ be defined as in Section 2.1. In dealing with multi-direction derivatives, we introduce the notation

$$\mathbf{x}^{\alpha,q} = x_1^{\alpha_1}, \dots, x_d^{\alpha_d}, x_{d+1}^q, \quad \text{with } \mathbf{x} \in \mathbb{R}^{d+1}, \quad q \in \mathbb{N}_0, \quad (3.7a)$$

$$D_{\Phi_n}^{\boldsymbol{\alpha}} f = \frac{\partial^{\alpha_1}}{\partial \mathbf{g}_{n,1}^{\alpha_1}} \cdots \frac{\partial^{\alpha_d} f}{\partial \mathbf{g}_{n,d}^{\alpha_d}}, \quad D_{\Phi_n}^{\boldsymbol{\alpha},q} f = \frac{\partial^{\alpha_1}}{\partial \mathbf{g}_{n,1}^{\alpha_1}} \cdots \frac{\partial^{\alpha_d} f}{\partial \mathbf{g}_{n,d}^{\alpha_d}} \frac{\partial^{\alpha_q} f}{\partial \mathbf{g}_{n,d+1}^{\alpha_q}}. \quad (3.7b)$$

In relation to the $D_{\Phi_n}^{\boldsymbol{\alpha},q} f$ derivatives, we define the norms and seminorms

$$\begin{aligned} \|f\|_{\mathcal{H}_{\Phi_n}^{\boldsymbol{\alpha},q}(Q_n)}^2 &= \sum_{s_1=0}^{\alpha_1} \cdots \sum_{s_d=0}^{\alpha_d} \sum_{s_{d+1}=0}^q |f|_{\mathcal{H}_{\Phi_n}^{\boldsymbol{\alpha},q}(Q_n)}^2, \\ |f|_{\mathcal{H}_{\Phi_n}^{\boldsymbol{\alpha},q}(Q_n)}^2 &= \sum_{E \in T_{h_n, Q_n}^{(n)}} |f|_{H_{\Phi_n}^{\boldsymbol{\alpha},q}(E)}^2, \end{aligned} \quad (3.8)$$

where

$$|f|_{H_{\Phi_n}^{\boldsymbol{\alpha},q}(E)}^2 = \|D_{\Phi_n}^{\boldsymbol{\alpha},q} f\|_{L_2(E)}^2.$$

We introduce the space $H_{\Phi_n}^{\boldsymbol{\alpha},q}(Q_n)$ endowed with the norm $\|\cdot\|_{H_{\Phi_n}^{\boldsymbol{\alpha},q}(Q_n)} = \|\cdot\|_{\mathcal{H}_{\Phi_n}^{\boldsymbol{\alpha},q}(Q_n)}$. Below, we show the relation between the $\mathbf{g}_{n,i}$ directional derivative norms and norms of the usual partial derivatives.

Proposition 3.1. *Let $f : Q \rightarrow \mathbb{R}$ be a smooth function and let the Assumption 2.3 and the multi-index $\boldsymbol{\alpha}$ such that $|\boldsymbol{\alpha}| = 1$. For all $E \in T_{h_n, Q_n}^{(n)}$ we have the relations*

$$\|D^{\boldsymbol{\alpha}} f\|_{L_2(E)} \sim \sum_{|\boldsymbol{\alpha}|=1} \|D_{\Phi_n}^{\boldsymbol{\alpha},0} f\|_{L_2(E)}, \quad (3.9a)$$

$$\|f\|_{H^{\ell,m}(E)} \sim \sum_{|\boldsymbol{\alpha}|=1} \|f\|_{\mathcal{H}_{\Phi_n}^{\boldsymbol{\alpha},m}(E)}, \quad (3.9b)$$

where the associated constants depend on $p, \gamma, \mathbf{g}_{n,i}$ and Φ_n .

Proof. The inequalities (3.9) follow by definition (3.8) and (3.6). ■

Assumption 3.1 *For simplicity, we assume that $p+1 \geq \max(\ell, m)$, cf. Assumption 2.1.*

Theorem 3.1. *Let the multi-index $\boldsymbol{\alpha}$ such that $|\boldsymbol{\alpha}| = 1$. Let the Assumptions 2.2, 2.3 and 3.1 hold and let $E \in T_{h_n, Q_n}^{(n)}$ and \tilde{E} be its support extension. Furthermore, let $f \in H^{\ell,m}(Q_n)$ with $\ell \geq 2$ and $m \geq 1$. Then, the quasi-interpolation estimates*

$$\left(\sum_{E \in T_{h_n, Q_n}^{(n)}} |\nabla_x (f - \Pi_h^{(n)} f)|_{L_2(E)}^2 \right)^{\frac{1}{2}} \leq C_x (h_n^{\ell-1} + h_n^m) \|f\|_{H^{\ell,m}(Q_n)}, \quad (3.10a)$$

$$\left(\sum_{E \in T_{h_n, Q_n}^{(n)}} |\partial_t (f - \Pi_h^{(n)} f)|_{L_2(E)}^2 \right)^{\frac{1}{2}} \leq C_t (h_n^{\ell} + h_n^{m-1}) \|f\|_{H^{\ell,m}(Q_n)}, \quad (3.10b)$$

$$\left(\sum_{E \in T_{h_n, Q_n}^{(n)}} |f - \Pi_h^{(n)} f|_{L_2(E)}^2 \right)^{\frac{1}{2}} \leq C_0 (h_n^{\ell} + h_n^m) \|f\|_{H^{\ell,m}(Q_n)}, \quad (3.10c)$$

holds, with C_x, C_t and C_0 depending only on $d, p, \gamma, \mathbf{g}_{n,i}$ and Φ_n .

Proof. We noted above that the last component of $\mathbf{g}_{n,i}$ is equal to zero. This implies that the derivatives $\frac{\partial f(x,t)}{\partial \mathbf{g}_{n,i}}$, see (3.6), do not include terms like $\frac{\partial f}{\partial t}$. Since $f \in H^{\ell,m}(Q)$, we have that $f \in H_{\Phi_n}^{\ell\alpha,0}(Q_n) \cap H_{\Phi_n}^{0,m}(Q_n)$, where α is a multi-index with d -components such that $|\alpha| = 1$. Making use of the interpolation results presented in [10], see Theorem 4.18, we have

$$\|D_{\Phi_n}^{\alpha,0}(f - \Pi_h^{(n)} f)\|_{L_2(E)} \leq c_1 \left(h_n^{\ell-1} + h_n^m \right) \sum_{|\alpha|=1} \|f\|_{\mathcal{H}_{\Phi_n}^{\ell\alpha,m}(\tilde{E})}. \quad (3.11)$$

Using (3.9) and (3.11), we can derive the following interpolation estimate

$$\|\nabla_x(f - \Pi_h^{(n)} f)\|_{L_2(E)} \leq c_2 \sum_{|\alpha|=1} \|D_{\Phi_n}^{\alpha,0}(f - \Pi_h^{(n)} f)\|_{L_2(E)} \leq c_3 \left(h_n^{\ell-1} + h_n^m \right) \|f\|_{H^{\ell,m}(\tilde{E})}, \quad (3.12)$$

with c_2 and c_3 depending on d, p, γ, Φ_n . In (3.12) summing over all $E \in T_{h_n, Q_n}^{(n)}$, we have that

$$\begin{aligned} \sum_E \|\nabla_x(f - \Pi_h^{(n)} f)\|_{L_2(E)}^2 &\leq c_4 \left(h_n^{\ell-1} + h_n^m \right)^2 \sum_E \|f\|_{H^{\ell,m}(\tilde{E})}^2, \\ &\leq c_5 \left(h_n^{\ell-1} + h_n^m \right)^2 \sum_E \sum_{E' \in \tilde{E}} \|f\|_{H^{\ell,m}(E')}^2 \end{aligned} \quad (3.13)$$

where c_4 and c_5 depend on the constant c_3 . Now, we observe that the last double sum in (3.13) consists of repeated element norm terms as $\|f\|_{H^{\ell,m}(E)}$. More precisely, for every element $E \in T_{h_n, Q_n}^{(n)}$, the related norm term $\|f\|_{H^{\ell,m}(E)}$ appears as many times in (3.13) as the number of the extension supports \tilde{E} , lets say $E_{Nb, \tilde{E}}$, where the element E belongs. By the constructing nature of B-splines, $E_{Nb, \tilde{E}}$ depends on the underlying B-spline degree and the knot repetitions m_i , i.e., the smoothness of B-splines across the microelement interfaces. Setting $E_{max, \tilde{E}} = \max_{E \in T_{h_n, Q_n}^{(n)}} \{E_{Nb, \tilde{E}}\}$, inequality (3.13) gives

$$\begin{aligned} \sum_E \|\nabla_x(f - \Pi_h^{(n)} f)\|_{L_2(E)}^2 &\leq c_5 E_{max, \tilde{E}} \left(h_n^{\ell-1} + h_n^m \right)^2 \|f\|_{H^{\ell,m}(E)}^2 \\ &\leq C_x^2 \left(h_n^{\ell-1} + h_n^m \right)^2 \|f\|_{H^{\ell,m}(Q_n)}^2, \end{aligned} \quad (3.14)$$

and estimate (3.10a) follows. Following similar procedure, we can show the estimates (3.10b) and (3.10c). \blacksquare

Proposition 3.2. *Let $\ell \geq 2$ and $m \geq 1$ be integers and let $f \in H^{\ell,m}(Q)$. Let the Assumptions 2.2, 2.3 and 3.1 hold, furthermore let $\Pi_h^n f$ be the corresponding quasi-interpolant defined above. Then there exist constants $C_i^*, i = 1, 2$ independent of f and h but dependent on the constants of (2.23) and on (3.10) such that*

$$\|f - \Pi_h^{(n)} f\|_{L_2(\partial Q_n)} \leq C_1^* \left(h_n^{\ell-\frac{1}{2}} + h_n^{m-\frac{1}{2}} \right) \|f\|_{H^{\ell,m}(Q_n)}, \quad (3.15a)$$

$$\|f - \Pi_h f\|_{dG,*} \leq C_2^* \left(h_n^{\ell-1} + h_n^{m-\frac{1}{2}} \right) \|f\|_{H^{\ell,m}(Q)}. \quad (3.15b)$$

Proof. Using the trace inequalities given in (2.23) and then (3.10), we have that

$$\begin{aligned} \|f - \Pi_h^{(n)} f\|_{L_2(\partial Q_n)}^2 &\leq C_{tr} \left(h_n^{-1} \left(\|f - \Pi_h^{(n)} f\|_{L_2(Q_n)}^2 + h_n \|\nabla f - \nabla \Pi_h^{(n)} f\|_{L_2(Q_n)}^2 \right) \right) \\ &\leq C_1^* \left(h_n^{2(\ell-\frac{1}{2})} + h_n^{2(m-\frac{1}{2})} \right) \|f\|_{H^{\ell,m}(Q_n)}^2. \end{aligned} \quad (3.16)$$

Recalling the definition of $\|\cdot\|_{dG,*}$ and using again the estimates (3.10) and (3.15a), we obtain

$$\begin{aligned}
\|f - \Pi_h f\|_{dG,*}^2 &= \left(\sum_{n=1}^N \left(\|\nabla_x f - \Pi_h^{(n)} f\|_{L_2(Q_n)}^2 + \theta h \|\partial_t f - \Pi_h^{(n)} f\|_{L_2(Q_n)}^2 \right. \right. \\
&\quad \left. \left. + \frac{1}{2} \|\llbracket (f - \Pi_h f)^{n-1} \rrbracket\|_{L_2(\Sigma_{n-1})}^2 \right) + \frac{1}{2} \|f - \Pi_h^{(N)} f\|_{L_2(\Sigma_N)}^2 \right) \\
&\quad + \sum_{n=1}^N (\theta_n h)^{-1} \|f - \Pi_h^{(n)} f\|_{L_2(Q_n)}^2 + \sum_{n=2}^N \|(f - \Pi_h^{(n-1)} f)^{n-1}\|_{L_2(\Sigma_{n-1})}^2 \\
&\leq \sum_{n=1}^N \left(C_{0,n} (h_n^{2(\ell-1)} + h_n^{2(m-\frac{1}{2})}) + C_{1,n} (h_n^{2(\ell-\frac{1}{2})} + h_n^{2(m-\frac{1}{2})}) + C_{2,n} (\theta_n h_n)^{-1} (h_n^{2\ell} + h_n^{2m}) \right) \|f\|_{H^{\ell,m}(Q_n)}^2 \\
&\leq \sum_{n=1}^N \left((C_{0,n} + C_{1,n} + C_{2,n}) \left(h_n^{2(\ell-1)} + \theta_n h_n^{2\ell-1} + h_n^{2m-1} + \theta_n h_n^{2m-1} \right) \|f\|_{H^{\ell,m}(Q_n)}^2 \right) \\
&\leq C_2^* (h^{2(\ell-1)} + h^{2(m-\frac{1}{2})}) \|f\|_{H^{\ell,m}(Q)}^2, \quad (3.17)
\end{aligned}$$

where a reduction of the terms $h^{\ell-1}$ and $h^{\ell-\frac{1}{2}}$ have been performed. This completes the proof of (3.15b). \blacksquare

Theorem 3.2. *Let u and u_h solve (2.7) and (2.22a), respectively. and u_h solve (2.22a).*

Under Assumption 2.1, there exist a $c > 0$, independent of h such that

$$\|u - u_h\|_{dG} \leq c(h^{\ell-1} + h^{m-\frac{1}{2}}) \|u\|_{H^{\ell,m}(\Omega)}, \quad (3.18)$$

Moreover, if $1 \leq m < \ell \leq p + 1$

$$\|u - u_h\|_{dG} \leq c h^{m-\frac{1}{2}} \|u\|_{H^{\ell,m}(\Omega)}. \quad (3.19)$$

Proof. Using the properties of bilinear form $a_h(\cdot, \cdot)$, i.e., V_{0h} ellipticity and the boundedness, as well as the consistency (2.35), we can obtain

$$\|u_h - \Pi_h u\|_{dG}^2 \leq c_1 a_h(u_h - \Pi_h u, u_h - \Pi_h u) = a_h(u - \Pi_h u, u_h - \Pi_h u) \leq c_2 \|u - \Pi_h u\|_{dG,*} \|u_h - \Pi_h u\|_{dG}. \quad (3.20)$$

Hence, applying triangle inequality $\|u - u_h\|_{dG} \leq \|u - \Pi_h u\|_{dG,*} + \|u_h - \Pi_h u\|_{dG}$, we can derive

$$\|u - u_h\|_{dG} \leq c \|u - \Pi_h u\|_{dG,*}. \quad (3.21)$$

Utilizing the estimate (3.15) in (3.21) yields (3.18). Estimate (3.19) is a direct result of (3.18). \blacksquare

Remark 3.1. We remark that for the case of highly smooth solutions, i.e., $p + 1 \leq \min(\ell, m)$, the estimate (3.18) takes the form

$$\|u - u_h\|_{dG} \leq c h^p \|u\|_{H^{\ell,m}(\Omega)}. \quad (3.22)$$

4 Matrix representation and space-time multigrid

We recall the discrete variational problem given in (2.22a), where we want to find $u_h \in V_{0h}$ such that

$$a_h(u_h, v_h) = l_h(v_h), \quad \forall v_h \in V_{0h},$$

with $V_{0h} := V_h^{(1)} \times \dots \times V_h^{(N)}$ and

$$a_h(u_h, v_h) = \sum_{n=1}^N a_{Q_n}(u_h^n, v_h^n),$$

where the local bilinear form for each space-time patch $n = 1, \dots, N$ is given by

$$\begin{aligned} a_{Q_n}(u_h^n, v_h^n) &= \int_{Q_n} \partial_t u_h^n (v_h^n + \theta_n h_n \partial_t v_h^n) + \nabla_x u_h^n \cdot \nabla_x (v_h^n + \theta_n h_n \partial_t v_h^n) dx dt + \int_{\Sigma_{n-1}} \llbracket u_h \rrbracket^{n-1} v_{h,+}^{n-1} ds \\ &= \int_{Q_n} \partial_t u_h^n (v_h^n + \theta_n h_n \partial_t v_h^n) + \nabla_x u_h^n \cdot \nabla_x (v_h^n + \theta_n h_n \partial_t v_h^n) dx dt + \int_{\Sigma_{n-1}} u_{h,+}^{n-1} v_{h,+}^{n-1} ds \\ &\quad - \int_{\Sigma_{n-1}} u_{h,-}^{n-1} v_{h,+}^{n-1} ds \\ &=: b_{Q_n}(u_h^n, v_h^n) - \int_{\Sigma_{n-1}} u_{h,-}^{n-1} v_{h,+}^{n-1} ds. \end{aligned}$$

For the local spaces $V_h^{(n)}$, $n = 1, \dots, N$, we now introduce the basis functions

$$V_h^{(n)} = \text{span}\{\varphi_j^n\}_{j=1}^{N_n},$$

and we obtain from the discrete problem (2.22a) the linear system

$$\mathbf{L}_h \mathbf{u}_h := \begin{pmatrix} \mathbf{A}_1 & & & & \\ -\mathbf{B}_2 & \mathbf{A}_2 & & & \\ & & \ddots & \ddots & \\ & & & & -\mathbf{B}_N & \mathbf{A}_N \end{pmatrix} \begin{pmatrix} \mathbf{u}_1 \\ \mathbf{u}_2 \\ \vdots \\ \mathbf{u}_N \end{pmatrix} = \begin{pmatrix} \mathbf{f}_1 \\ \mathbf{f}_2 \\ \vdots \\ \mathbf{f}_N \end{pmatrix} =: \mathbf{f}_h, \quad (4.1)$$

with the matrices

$$\mathbf{A}_n[i, j] := b_{Q_n}(\varphi_j^n, \varphi_i^n) \quad \text{for } i, j = 1, \dots, N_n$$

on the diagonal for $n = 1, \dots, N$, and the matrices

$$\mathbf{B}_n[i, k] := \int_{\Sigma_{n-1}} \varphi_{k,-}^{n-1} \varphi_{i,+}^{n-1} ds \quad \text{for } k = 1, \dots, N_{n-1} \text{ and } i = 1, \dots, N_n.$$

on the lower off diagonal for $n = 2, \dots, N$. Moreover, the right hand sides are given by

$$\mathbf{f}_n[i] := l_h(\varphi_i^n), \quad i = 1, \dots, N_n,$$

for $n = 1, \dots, N$. The linear system (4.1) can be solved by solving the local space-time problems sequentially from one space-time patch to the next space-time patch, i.e., like a time stepping scheme

$$\mathbf{A}_n \mathbf{u}_n = \mathbf{f}_n + \mathbf{B}_n \mathbf{u}_{n-1} \quad \text{for } n = 2, \dots, N.$$

In this work, we will solve the linear system (4.1) by using a space-time multigrid approach similar to that one proposed in [19]. In particular, we use an (inexact) damped Jacobi scheme as smoother, i.e.,

$$\mathbf{u}_h^{k+1} = \mathbf{u}_h^k + \omega \mathbf{D}_h^{-1} [\mathbf{f}_h - \mathbf{L}_h \mathbf{u}_h^k] \quad \text{for } k = 1, 2, \dots,$$

where we use the block diagonal matrix $\mathbf{D}_h := \text{diag}\{\mathbf{A}_n\}_{n=1}^N$ and the damping parameter $\omega = \frac{1}{2}$, see also [19]. We speed up the application of the smoothing iteration by replacing the exact inverse of \mathbf{D}_h by some appropriate approximation. In detail, we will apply one iteration of an algebraic multigrid solver (hypr [17, 16]) with respect to the diagonal matrices \mathbf{A}_n , $n = 1, \dots, N$, i.e. for each single space-time patch Q_n . For the single patch case this type of solvers were successfully used in [35]. For the space-time multigrid approach, we construct a space-time hierarchy by

always combining two space-time patches to one coarser space-time patch, where we always apply standard coarsening in time and space direction. We then have all the components available for setting up a standard multigrid V-cycle. The advantage is that this method is fully parallel with respect to space and time, since we use an additive smoother in time direction and apply standard parallel solvers in space direction. Moreover, we will use one iteration of this space-time multigrid V-cycle as a preconditioner for the GMRES method.

If the IgA maps $\Phi_n : \widehat{Q} \rightarrow Q_n, n = 1, \dots, N$, preserve the tensor product structure of the IgA basis functions φ_i^n , we can use this information to save assembling time and storage costs for the linear system (4.1). In this case we can write the basis functions φ_i^n in the form

$$\varphi_i^n(x, t) = \phi_{i_x}^n(x) \psi_{i_t}^n(t) \quad \text{with } i_x \in \{1, \dots, N_{n,x}\} \text{ and } i_t \in \{1, \dots, N_{n,t}\},$$

with $N_n = N_{n,x}N_{n,t}$. Using this representation, we can write the matrices $\mathbf{A}_n, n = 1, \dots, N$ as

$$\mathbf{A}_n = \mathbf{M}_{n,x} \otimes \mathbf{K}_{n,t} + \mathbf{K}_{n,x} \otimes \mathbf{M}_{n,t},$$

with the standard mass and stiffness matrices with respect to space

$$\mathbf{M}_{n,x}[i_x, j_x] := \int_{\Omega} \phi_{j_x}^n \phi_{i_x}^n dx, \quad \mathbf{K}_x[i_x, j_x] := \int_{\Omega} \nabla_x \phi_{j_x}^n \cdot \nabla_x \phi_{i_x}^n dx,$$

where $i_x, j_x = 1, \dots, N_{n,x}$ and corresponding matrices with respect to time

$$\begin{aligned} \mathbf{K}_{n,t}[i_t, j_t] &:= \int_{t_{n-1}}^{t_n} \partial_t \psi_{j_t}^n (\psi_{i_t}^n + \theta_n h_n \partial_t \psi_{i_t}^n) dt + \psi_{j_t}^n(t_{n-1}) \psi_{i_t}^n(t_{n-1}), \\ \mathbf{M}_{n,t}[i_t, j_t] &:= \int_{t_{n-1}}^{t_n} \psi_{j_t}^n (\psi_{i_t}^n + \theta_n h_n \partial_t \psi_{i_t}^n) dt, \end{aligned}$$

with $i_t, j_t = 1, \dots, N_{n,t}$. The matrices on the off diagonal $\mathbf{B}_n, n = 2, \dots, N$, can be written in the form

$$\mathbf{B}_n := \widetilde{\mathbf{M}}_{n,x} \otimes \mathbf{N}_{n,t},$$

with the matrices

$$\widetilde{\mathbf{M}}_{n,x}[i_x, k_x] := \int_{\Omega} \phi_{k_x}^{n-1} \phi_{i_x}^n dx \quad \text{and} \quad \mathbf{N}_{n,t}[i_t, k_t] := \psi_{k_t}^{n-1}(t_{n-1}) \psi_{i_t}^n(t_{n-1}),$$

where $i_x = 1, \dots, N_{n,x}, k_x = 1, \dots, N_{n-1,x}, i_t = 1, \dots, N_{n,t}$ and $k_t = 1, \dots, N_{n-1,t}$.

5 Numerical examples

In the following, we present numerical examples supporting the theory developed in this paper. In Section 5.1, we verify the a-priori error estimate from Theorem 3.2 for higher order B-Splines. In Section 5.2, we show the parallel performance of the space-time solver given in Section 4.

5.1 Convergence studies

In this example, the problem is considered on the two dimensional space-time cylinder $Q = \Omega \times (0, 4)$ with $\Omega = (0, 1)$. We choose homogeneous boundary conditions and the source function

$$f(x, t) = \pi \sin(\pi x) \left(\frac{1}{2} \cos\left(\frac{\pi}{2}(t+1)\right) + \pi \sin\left(\frac{\pi}{2}(t+1)\right) \right).$$

Hence, the exact solution is given by

$$u(x, t) = \sin(\pi x) \sin\left(\frac{\pi}{2}(t + 1)\right). \quad (5.1)$$

The space-time cylinder Q is decomposed into four space-time patches $Q_n = \Omega \times (t_{n-1}, t_n)$ where $\{t_0, t_1, t_2, t_3, t_4\} = \{0, 1, 2, 3, 4\}$, see Fig. 2(a). The problem has been solved on a sequence of meshes with $h_0, \dots, h_i, h_{i+1}, \dots$, with $h_i = 2^{-i}$. According to Fig. 2(a), the mesh on Q_1 and Q_3 has one additional refinement. We discretize the problem using B-Splines of degree $p = \{2, 3, 4\}$. Throughout all tests, θ_n is chosen to be 1 for all patches. The final linear system (4.1) is solved by means of a direct solver, where we used the PARDISO 5.0.0 Solver Project [46, 45]. The algorithm is realized in the isogeometric open source C++ library G+SMO [39]. The solution u_h on a coarse mesh with $h = 0.25$ is visualized in Fig. 2(a). The error in the dG-norm and the convergence rates are presented in Table 1 and plotted in Fig. 2(b).

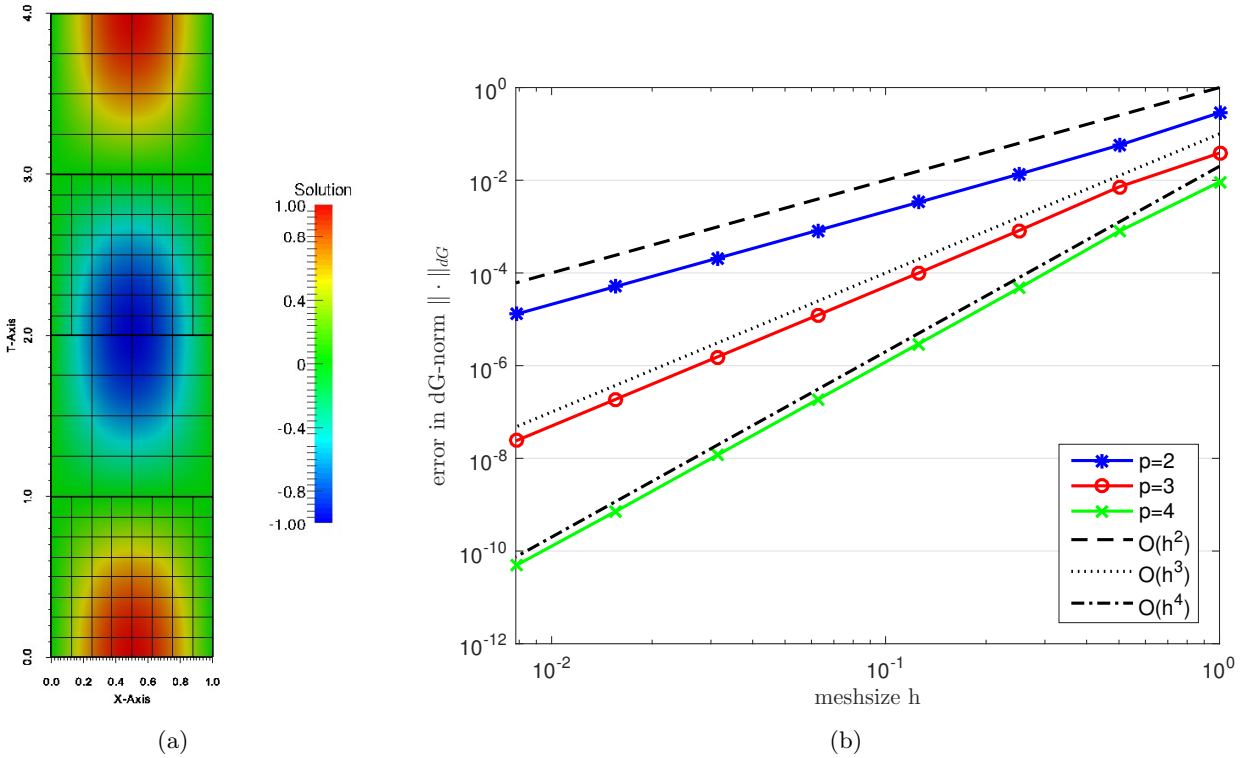


Fig. 2. (a) The solution u_h on Q having non-matching meshes across the interface after two uniform refinements of the initial mesh. (b) Convergence plots for polynomial degrees $p = \{2, 3, 4\}$.

refinement	$p = 2$		$p = 3$		$p = 4$	
	error	eoc	error	eoc	error	eoc
0	2.85633E-02	-	3.85617E-02	-	9.18731E-03	-
1	5.68232E-02	2.33	7.15551E-03	2.43	7.87619E-04	3.54
2	1.34212E-02	2.08	8.11296E-04	3.14	4.62549E-05	4.09
3	3.30721E-03	2.02	9.84754E-05	3.04	2.90675E-06	3.99
4	8.23704E-04	2.01	1.22142E-05	3.01	1.84067E-07	3.98
5	2.05716E-04	2.00	1.52376E-06	3.00	1.16139E-08	3.99
6	5.14138E-05	2.00	1.90375E-07	3.00	7.29917E-10	3.99
7	1.28522E-05	2.00	2.37936E-08	3.00	4.85647E-11	3.91

Table 1. Error in the dG-norm and convergence rate for B-Spline degree 2, 3 and 4.

We observe that the obtained convergence rates coincide with the theoretically predicted rates from Theorem 3.2 for smooth solutions u . To be more precise, we observe $\|u - u_h\|_{dG}$ behaves like $O(h^p)$, where p is the B-Spline degree.

5.2 Parallel solver studies

Here we apply the parallel multigrid solver that was introduced in Section 4 to solve the arising linear systems for the case $p = 1$, i.e., for lowest order splines. In detail, we consider the simulation time $T = 1$ and the computational domain $\Omega \subset \mathbb{R}^3$ given by the control points

$$\left\{ (0, 0, 0)^\top, (1, 0, 0)^\top, (1, 1, 0)^\top, (0, 1, 0)^\top, \left(-\frac{1}{4}, -\frac{1}{4}, 1\right)^\top, (1, 0, 1)^\top, (1, 1, 1)^\top, \left(-\frac{1}{4}, \frac{5}{4}, 1\right)^\top \right\},$$

see also Figure 3.

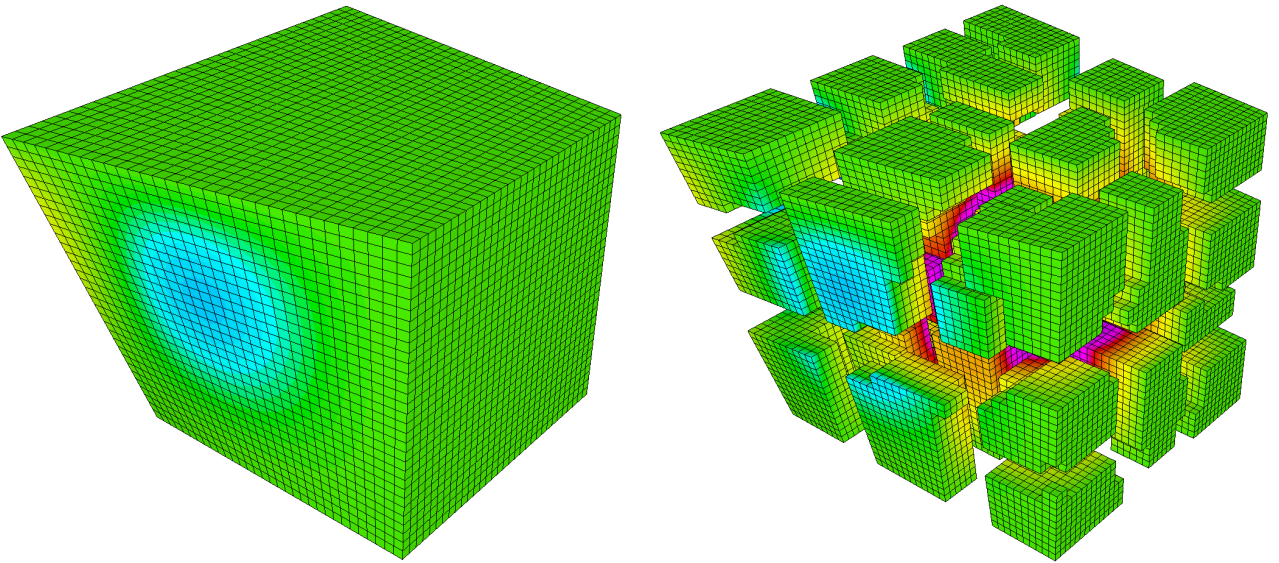


Fig. 3. Computational spatial domain Ω decomposed into 4096 elements (left) and distributed over 32 processors (right). The numerical solution given in Table 2 is plotted at $t = 0.5$.

For the initial space-time, mesh we use one space-time patch ($N = 1$) which is decomposed into 64 elements in space and 8 elements wrt time. We then apply uniform refinement wrt to space, and, at the same time, we increase the number of space-time patches by a factor of two, i.e. uniform refinement in space and time. Throughout all computations we use the parameter $\theta_n = 0.2$ for all space-time patches. Moreover, we assemble the linear systems and apply the parallel space-time multigrid solver, discussed in Section 4, as a preconditioner for the GMRES method. For the problem in space, we make use of the software library MFEM [40], where the AMG library *hypr* is used as parallel solver in space. For the time parallelization, we use the software developed in [19]. For all examples, we stop the GMRES method until a relative residual error of 10^{-12} is reached. In Table 2, we present the numerical results for the manufactured solution

$$u(x, t) = \sin(\pi x_1) \sin(\pi x_2) \sin(\pi x_3) \sin(\pi t),$$

which is regular. For this example, we observe the optimal convergence rates in the dG-norm, which is predicted by the theory given in Theorem 3.2. For the $L_2(Q)$ -norm, we also obtain the optimal rates. Furthermore, we also obtain quite small iteration numbers for the preconditioned GMRES method. In Table 2, we denote the number of cores which are used for the *hypr* AMG solver and the number of cores which are used for the time parallelization by c_x and c_t , respectively. Hence, we use $c_x c_t$ cores overall. Finally, we can solve a linear system consisting of 9 777 365 568

N	dof per patch	overall dof	$\ u - u_h\ _{L_2(Q)}$ eoc	$\ u - u_h\ _{dG}$ eoc	c_x	c_t	cores	iter	time [s]
1	1 125	1 125	2.41829E-02	-	3.56223E-01	-	1 1	1 1	0.03
2	6 561	13 122	6.27531E-03	1.95	1.77477E-01	1.01	1 2	2 13	1.87
4	44 217	176 868	1.58802E-03	1.98	8.86255E-02	1.00	1 4	4 15	21.47
8	323 433	2 587 464	3.98310E-04	2.00	4.42868E-02	1.00	4 8	32 15	100.48
16	2 471 625	39 546 000	9.96216E-05	2.00	2.21376E-02	1.00	32 16	512 17	94.32
32	19 320 201	618 246 432	2.49008E-05	2.00	1.10675E-02	1.00	256 32	8192 17	162.90
64	152 771 337	9 777 365 568	6.22393E-06	2.00	5.53340E-03	1.00	2048 64	131072 17	211.33

Table 2. Convergence results in the $L_2(Q)$ -norm and dG-norm for a regular solution as well as iteration numbers and solving times for the parallel space-time multigrid preconditioned GMRES method.

unknowns in less than 4 minutes. We also observe a reasonable weak parallel efficiency of at least 75%, which is mainly affected by the efficiency of the parallel AMG solver *hypre*.

In Table 3, we give the convergence rates for the manufactured solution

$$u(x, t) = \sin(\pi x_1) \sin(\pi x_2) \sin(\pi x_3) (1 - t)^\alpha \in H^{s, \alpha + \frac{1}{2} - \varepsilon}(Q)$$

for $\alpha = 0.75$, for an arbitrary $s \geq 2$ and for an arbitrary small $\varepsilon > 0$, which has lower regularity wrt time, see also [43]. By Theorem 3.2, the asymptotic convergence rate wrt h is then (almost) given by 0.75. In Table 3, we observe a convergence rate of one, since we are still in the pre-asymptotic range. For the $L_2(Q)$ -error, we obtain a reduced convergence rate, which will be 1.25 in the asymptotic range. We also observe that the solver is not effected at all by the regularity of the solution.

N	dof per patch	overall dof	$\ u - u_h\ _{L_2(Q)}$ eoc	$\ u - u_h\ _{dG}$ eoc	c_x	c_t	cores	iter	time [s]
1	1 125	1 125	1.96957E-02	-	3.15855E-01	-	1 1	1 1	0.03
2	6 561	13 122	5.06642E-03	1.96	1.58494E-01	0.99	1 2	2 13	1.86
4	44 217	176 868	1.27969E-03	1.99	7.92759E-02	1.00	1 4	4 15	21.46
8	323 433	2 587 464	3.24639E-04	1.98	3.96365E-02	1.00	4 8	32 15	100.49
16	2 471 625	39 546 000	8.44577E-05	1.94	1.98187E-02	1.00	32 16	512 17	94.35
32	19 320 201	618 246 432	2.33578E-05	1.85	9.91105E-03	1.00	256 32	8192 17	163.01
64	152 771 337	9 777 365 568	7.20492E-06	1.70	4.95723E-03	1.00	2048 64	131072 17	211.47

Table 3. Convergence results in the $L_2(Q)$ -norm and dG-norm for a low regularity solution as well as iteration numbers and solving times for the parallel space-time multigrid preconditioned GMRES method.

In the next example, we use a different manufactured solution

$$u(x, t) = \cos(\beta x_1) \cos(\beta x_2) \cos(\beta x_3) (1 - t)^\alpha \in H^{s, \alpha + \frac{1}{2} - \varepsilon}(Q)$$

for $\alpha = 0.75$ and $\beta = 0.3$, for an arbitrary $s \geq 2$, and for an arbitrary small $\varepsilon > 0$, which has the same regularity as the solution from the previous example. In Table 4, we observe the expected convergence rates predicted by Theorem 3.2.

All parallel computations have been performed on the cluster Vulcan BlueGene/Q at Livermore, U.S.A.

6 Conclusions

We have presented and analyzed a time-multipatch discontinuous Galerkin space-time IgA method for solving initial-boundary value problems for linear parabolic partial differential equations. The method proposed uses discontinuous Galerkin techniques with time-upwind fluxes for establishing the communication of the discrete solution across the time patch interfaces. Furthermore, time-upwind diffusion techniques was used for stabilizing the time discretization within each patch.

N	dof per patch	overall dof	$\ u - u_h\ _{L_2(Q)}$ eoc	$\ u - u_h\ _{dG}$ eoc	c_x	c_t	cores	iter	time [s]
1	1 125	1 125	7.10407E-03	-	1.58022E-02	-	1 1	1 1	0.03
2	6 561	13 122	2.66063E-03	1.42	8.88627E-03	0.83	1 2	2 13	2.00
4	44 217	176 868	1.00177E-03	1.41	5.41668E-03	0.71	1 4	4 15	21.48
8	323 433	2 587 464	3.78976E-04	1.40	3.33881E-03	0.70	4 8	32 15	100.57
16	2 471 625	39 546 000	1.44246E-04	1.39	2.05545E-03	0.70	32 16	512 17	94.43
32	19 320 201	618 246 432	5.53509E-05	1.38	1.25859E-03	0.71	256 32	8192 17	171.83
64	152 771 337	9 777 365 568	2.14541E-05	1.37	7.65921E-04	0.72	2048 64	131072 17	211.49

Table 4. Convergence results in the $L_2(Q)$ -norm and dG-norm for a low regularity solution as well as iteration numbers and solving times for the parallel space-time multigrid preconditioned GMRES method.

A complete discretization error analysis was developed in a suitable energy norm including the case where the solution can exhibit different regularity behavior with respect the space and time directions. The convergence rate estimates were confirmed by numerical experiments. We proposed fast techniques for generating and solving the huge system of IgA equations on massively parallel computers. The parallel experiments were performed for a 3d spatial domain Ω yielding a 4d space-time cylinder $Q = \Omega \times (0, T)$ but only for the case $p = 1$ where the IgA coincides with the FEM. In this paper, we always assumed that the spatial computational domain Ω has a singlepatch representation. The multipatch representation of Ω , which is more important in practice, in connection with dG coupling in space [37] and Dual-Primal Isogeometric Tearing and Interconnection (IETI-DP) solution techniques [22, 21] is work in progress. This approach is quite flexible with respect to the adaption of the discretization to the behavior of the solution. At the same, it allows a fast generation and solution of the system of IgA equations due to the fact that the local space-time patches into which the space-time cylinder Q is decomposed have still tensor product structure. A complete unstructured decomposition of the space-time cylinder Q into patches, which was considered in [42], loses this structure, and, therefore, an efficient implementation is cumbersome.

Acknowledgments

This work was supported by the Austrian Science Fund (FWF) under the grants NFN S117-03 and DK W1214-04.

References

1. R. Andreev. Stability of sparse space-time finite element discretizations of linear parabolic evolution equations. *IMA J. Numer. Anal.*, 33(1):242–260, 2013.
2. R. Andreev, O. Scherzer, and W. Zulehner. Simultaneous optical flow and source estimation: Spacetime discretization and preconditioning. *Applied Numerical Mathematics*, 96:72–81, 2015.
3. I. Babuška and T. Janik. The h-p version of the finite element method for parabolic equations. Part I. the p-version in time. *Numerical Methods for Partial Differential Equations*, 5(4):363–399, 1989.
4. I. Babuška and T. Janik. The h-p version of the finite element method for parabolic equations. II. the h-p version in time. *Numerical Methods for Partial Differential Equations*, 6(4):343–369, 1990.
5. R. E. Bank, P. S. Vassilevski, and L. T. Zikatanov. Arbitrary dimension convection–diffusion schemes for space–time discretizations. *Journal of Computational and Applied Mathematics*, 310:19–31, 2017.
6. R.E. Bank and M.S. Metti. An error analysis of some higher order space-time moving finite elements. *Comput Visual Sci*, 16:219–229, 2013.
7. Y. Bazilevs, L. Beirao da Veiga, J. A. Cottrell, T.J.R. Hughes, and G. Sangalli. Isogeometric analysis: approximation, stability and error estimates for h -refined meshes. *Math. Mod. Meth. Appl. Sci.*, 16(7):1031–1090, 2006.
8. M. Behr. Simplex space-time meshes in finite element simulations. *Internat. J. Numer. Methods Fluids*, 57:1421–1434, 2008.
9. L. Beirao da Veiga, A. Buffa, J. Rivas, and G. Sangalli. Some estimates for h - p - k refinement in Isogeometric Analysis. *Numerische Mathematik*, 118(7):271–305, 2011.
10. L. Beirao da Veiga, A. Buffa, G. Sangalli, and R. Vázquez. Mathematical analysis of variational isogeometric methods. *Acta Numerica*, 23:157–287, 5 2014.
11. L. Beirao da Veiga, D. Cho, and G. Sangalli. Anisotropic NURBS approximation in isogeometric analysis. *Comput. Methods Appl. Mech. Engrg.*, 209-212:1–11, 2012.

12. D. Braess. *Finite Elements: Theory, Fast Solvers, and Applications in Solid Mechanics*. Cambridge University, United Kingdom, 3rd edition, 2007.
13. J. A. Cottrell, T.J.R. Hughes, and Y. Bazilevs. *Isogeometric Analysis, Toward Integration of CAD and FEA*. John Wiley and Sons, 2009.
14. C. De-Boor. *A Practical Guide to Splines*, volume 27 of *Applied Mathematical Science*. Springer, New York, revised edition, 2001.
15. J. Evans and T. J.R. Hughes. Explicit trace inequalities for isogeometric analysis and parametric hexahedral finite elements. *Numerische Mathematik*, 123(2):259–290, 2013.
16. R.D. Falgout, J.E. Jones, and U.M. Yang. The design and implementation of hypre, a library of parallel high performance preconditioners. *Lect. Notes Comput. Sci. Eng.*, 51:267–294, 2006.
17. R.D. Falgout and U.M. Yang. hypre: A Library of High Performance Preconditioners. *Proceedings of the International Conference on Computational Science-Part III*, pages 632–641, 2002.
18. M. Gander. 50 years of time parallel time integration. In T. Carraro, M. Geiger, S. Körkel, and R. Rannacher, editors, *Multiple Shooting and Time Domain Decomposition*, pages 69–114. Springer-Verlag, 2015.
19. M. Gander and M. Neumüller. Analysis of a new space-time parallel multigrid algorithm for parabolic problems. *SIAM J. Sci. Comput.*, 38(4):A2173–A2208, 2016.
20. P. Hansbo. Space-time oriented streamline diffusion methods for nonlinear conservation laws in one dimension. *Comm. Numer. Methods Engrg.*, 10(3):203–215, 1994.
21. C. Hofer. Parallelization of continuous and discontinuous galerkin dual-primal isogeometric tearing and interconnecting methods. *Computers & Mathematics with Applications*, 2017. published online at <https://doi.org/10.1016/j.camwa.2017.06.051>.
22. C. Hofer and U. Langer. Dual-primal isogeometric tearing and interconnecting solvers for multipatch dG-IgA equations. *Comput. Methods Appl. Mech. Engrg.*, 316:2–21, 2017.
23. K. Hölling. *Finite element methods with B-splines*. SIAM, Philadelphia USA, 2003.
24. T. J. R. Hughes and A. Brooks. Streamline upwind / Petrov-Galerkin formulation for convection dominated flows with particular emphasis on the incompressible navier-stokes equations. *Comp. Meth. Appl. Mech. Engrg.*, 32:199–259, 1982.
25. T.J.R. Hughes, J. A. Cottrell, and Y. Bazilevs. Isogeometric analysis : CAD, finite elements, NURBS, exact geometry and mesh refinement. *Comput. Methods Appl. Mech. Engrg.*, 194:4135–4195, 2005.
26. C. Johnson. *Numerical solution of partial differential equations by the finite element method*. Dover Publications, Inc., Mineola, NY, 2009. Reprint of the 1987 edition.
27. C. Johnson, U. Nävert, and J. Pitkäranta. Finite element methods for linear hyperbolic problems. *Comput. Methods Appl. Mech. Engrg.*, 45(1-3):285–312, 1984.
28. C. Johnson and J. Saranen. Streamline diffusion methods for the incompressible Euler and Navier-Stokes equations. *Math. Comp.*, 47(175):1–18, 1986.
29. E. Karabelas. *Space-time discontinuous Galerkin methods for cardiac electro-mechanics*. PhD thesis, Technische Universität Graz, 2015.
30. E. Karabelas and M. Neumüller. Generating admissible space-time meshes for moving domains in $(d + 1)$ -dimensions. NuMa-Report 2015-07, Johannes Kepler University Linz, Institute for Computational Mathematics, Linz, November 2015.
31. O. A. Ladyzhenskaya. *The Boundary Value Problems of Mathematical Physics*. Nauka, Moscow, 1973. In Russian. Translated in *Appl. Math. Sci.* 49, Springer, 1985.
32. O. A. Ladyzhenskaya, V. A. Solonnikov, and N. N. Uraltseva. *Linear and Quasilinear Equations of Parabolic Type*. Nauka, Moscow, 1967. In Russian. Translated in AMS, Providence, RI, 1968.
33. J. Lang. *Adaptive Multilevel Solution of Nonlinear Parabolic PDE Systems. Theory, Algorithm, and Applications*, volume 16 of *Lecture Notes in Computational Sciences and Engineering*. Springer Verlag, Heidelberg, Berlin, 2000.
34. U. Langer, S. Matculevich, and S. Repin. Functional type error control for stabilised space-time iga approximations to parabolic problems. In I. Lirkov and S. Margenov, editors, *Large-Scale Scientific Computing (LSSC 2017)*, Lecture Notes in Computer Science (LNCS). Springer-Verlag, 2017. accepted for publication, also available as RICAM Report 2017-14 at <https://www.ricam.oeaw.ac.at/files/reports/17/rep17-14.pdf>.
35. U. Langer, S. Moore, and M. Neumüller. Space-time isogeometric analysis of parabolic evolution equations. *Comput. Methods Appl. Mech. Engrg.*, 306:342–363, 2016.
36. U. Langer, M. Neumüller, and I. Touloupoulos. Multipatch space-time isogeometric analysis of parabolic diffusion problems. In I. Lirkov and S. Margenov, editors, *Large-Scale Scientific Computing (LSSC 2017)*, Lecture Notes in Computer Science (LNCS). Springer-Verlag, 2017. accepted for publication, also available as RICAM Report 2017-18 at <https://www.ricam.oeaw.ac.at/files/reports/17/rep17-18.pdf>.
37. U. Langer and I. Touloupoulos. Analysis of multipatch discontinuous Galerkin IgA approximations to elliptic boundary value problems. *Computing and Visualization in Science*, 17(5):217–233, 2015.
38. S. Larsson and M. Molten. Numerical solution of parabolic problems based on a weak space-time formulation. *Comput. Methods Appl. Math.*, 17(1):65–84, 2017.
39. A. Mantzaflaris et al. G+SMO (Geometry plus Simulation MOdules) v0.8.1. <http://gs.jku.at/gismo>, 2015.
40. MFEM, modular finite element methods. mfem.org.
41. C. Mollet. Stability of Petrov-Galerkin discretizations: Application to the space-time weak formulation for parabolic evolution problems. *Computational Methods in Applied Mathematics*, 14(2):231–255, 2014.
42. S. Moore. *Nonstandard Discretization Strategies In Isogeometric Analysis for Partial Differential Equations*. PhD thesis, Johannes Kepler University Linz, Linz, 2017.
43. M. Neumüller. *Space-Time Methods: Fast Solvers and Applications*, volume 20 of *Monographic Series TU Graz: Computation in Engineering and Science*. TU Graz, 2013.

44. M. Neumüller and O. Steinbach. Refinement of flexible space–time finite element meshes and discontinuous Galerkin methods. *Comput. Visual. Sci.*, 14:189–205, 2011.
45. C.G. Petra, O. Schenk, and M. Anitescu. Real-time stochastic optimization of complex energy systems on high-performance computers. *IEEE Computing in Science & Engineering*, 16(5):32–42, 2014.
46. C.G. Petra, O. Schenk, M. Lubin, and K. Gärtner. An augmented incomplete factorization approach for computing the Schur complement in stochastic optimization. *SIAM Journal on Scientific Computing*, 36(2):C139–C162, 2014.
47. L. Piegl and W. Tiller. *The NURBS Book*. Springer-verlag, Berlin, Heidelberg, 1997. 2nd edition.
48. L. L. Schumaker. *Spline Functions: Basic Theory*. Cambridge, University Press, third Edition edition, 2007.
49. C. Schwab and R. Stevenson. Space–time adaptive wavelet methods for parabolic evolution problems. *Math. Comput.*, 78:1293–1318, 2009.
50. I. Smears. Robust and efficient preconditioners for the discontinuous galerkin time-stepping method. *IMA J. Numer. Anal.*, 00:1–25, 2016.
51. O. Steinbach. Space-time finite element methods for parabolic problems. *Comput. Meth. Appl. Math.*, 15(4):551–566, 2015.
52. M. Stynes. Steady–state convection–diffusion problems. *Acta Numerica*, 14:445–508, 2005.
53. K. Takizawa, B. Henicke, A. Puntel, N. Kostov, and T.E. Tezduyar. Space-time techniques for computational aerodynamics modeling of flapping wings of an actual locust. *Computational Mechanics*, 50(6):743–760, 2012.
54. K. Takizawa, N. Kostov, A. Puntel, B. Henicke, and T.E. Tezduyar. Space-time computational analysis of bio-inspired flapping-wing aerodynamics of a micro aerial vehicle. *Computational Mechanics*, 50(6):761–778, 2012.
55. K. Takizawa, T.E. Tezduyar, S. McIntyre, N. Kostov, R. Kolesar, and C. Habluetzel. Space-time VMS computation of wind-turbine rotor and tower aerodynamics. *Computational Mechanics*, 53(1):1–15, 2014.
56. K. Takizawa and T.E. Tezduyar. Multiscale space-time fluid-structure interaction techniques. *Computational Mechanics*, 48(3):247–267, 2011.
57. K. Takizawa and T.E. Tezduyar. Space-time computation techniques with continuous representation in time (ST-C). *Computational Mechanics*, 53(1):91–99, 2014.
58. V. Thomeé. *Galerkin finite element methods for parabolic problems*, volume 25 of *Springer Series in Computational Mathematics*. Springer-Verlag Berlin Heidelberg, 2006.
59. I. Touloupoulos. Stabilized space-time finite element methods of parabolic evolution problems. RICAM Report 2017-19, Johann Radon Institute for Computational and Applied Mathematics, Austrian Academy of Sciences, Linz, 2017.
60. K. Urban and A. T. Patera. An improved error bound for reduced basis approximation of linear parabolic problems. *Math. Comput.*, 83:1599–1615, 2014.

Technical Reports of the Doctoral Program

“Computational Mathematics”

2017

- 2017-01** E. Buckwar, A. Thalhammer: *Importance Sampling Techniques for Stochastic Partial Differential Equations* January 2017. Eds.: U. Langer, R. Ramlau
- 2017-02** C. Hofer, I. Touloupoulos: *Discontinuous Galerkin Isogeometric Analysis for parametrizations with overlapping regions* June 2017. Eds.: U. Langer, V. Pillwein
- 2017-03** C. Hofer, S. Takacs: *Inexact Dual-Primal Isogeometric Tearing and Interconnecting Methods* June 2017. Eds.: B. Jüttler, V. Pillwein
- 2017-04** M. Neumüller, A. Thalhammer: *Combining Space-Time Multigrid Techniques with Multilevel Monte Carlo Methods for SDEs* June 2017. Eds.: U. Langer, E. Buckwar
- 2017-05** C. Hofer, U. Langer, M. Neumüller: *Time-Multipatch Discontinuous Galerkin Space-Time Isogeometric Analysis of Parabolic Evolution Problems* August 2017. Eds.: V. Pillwein, B. Jüttler

2016

- 2016-01** P. Gangl, U. Langer: *A Local Mesh Modification Strategy for Interface Problems with Application to Shape and Topology Optimization* November 2016. Eds.: B. Jüttler, R. Ramlau
- 2016-02** C. Hofer: *Parallelization of Continuous and Discontinuous Galerkin Dual-Primal Isogeometric Tearing and Interconnecting Methods* November 2016. Eds.: U. Langer, W. Zulehner
- 2016-03** C. Hofer: *Analysis of Discontinuous Galerkin Dual-Primal Isogeometric Tearing and Interconnecting Methods* November 2016. Eds.: U. Langer, B. Jüttler
- 2016-04** A. Seiler, B. Jüttler: *Adaptive Numerical Quadrature for the Isogeometric Discontinuous Galerkin Method* November 2016. Eds.: U. Langer, J. Schicho
- 2016-05** S. Hubmer, A. Neubauer, R. Ramlau, H. U. Voss: *On the Parameter Estimation Problem of Magnetic Resonance Advection Imaging* December 2016. Eds.: B. Jüttler, U. Langer
- 2016-06** S. Hubmer, R. Ramlau: *Convergence Analysis of a Two-Point Gradient Method for Nonlinear Ill-Posed Problems* December 2016. Eds.: B. Jüttler, U. Langer

2015

- 2015-01** G. Grasegger, A. Lastra, J. Rafael Sendra, F. Winkler: *A Solution Method for Autonomous First-Order Algebraic Partial Differential Equations in Several Variables* January 2015. Eds.: U. Langer, J. Schicho
- 2015-02** P. Gangl, U. Langer, A. Laurain, H. Meftahi, K. Sturm: *Shape Optimization of an Electric Motor Subject to Nonlinear Magnetostatics* January 2015. Eds.: B. Jüttler, R. Ramlau
- 2015-03** C. Fürst, G. Landsmann: *Computation of Dimension in Filtered Free Modules by Gröbner Reduction* May 2015. Eds.: P. Paule, F. Winkler
- 2015-04** A. Mantzaflaris, H. Rahkooy, Z. Zafeirakopoulos: *Efficient Computation of Multiplicity and Directional Multiplicity of an Isolated Point* July 2015. Eds.: B. Buchberger, J. Schicho
- 2015-05** P. Gangl, S. Amstutz, U. Langer: *Topology Optimization of Electric Motor Using Topological Derivative for Nonlinear Magnetostatics* July 2015. Eds.: B. Jüttler, R. Ramlau
- 2015-06** A. Maletzky: *Exploring Reduction Ring Theory in Theorema* August 2015. Eds.: B. Buchberger, W. Schreiner

Doctoral Program

“Computational Mathematics”

Director:

Prof. Dr. Peter Paule
Research Institute for Symbolic Computation

Deputy Director:

Prof. Dr. Bert Jüttler
Institute of Applied Geometry

Address:

Johannes Kepler University Linz
Doctoral Program “Computational Mathematics”
Altenbergerstr. 69
A-4040 Linz
Austria
Tel.: ++43 732-2468-6840

E-Mail:

office@dk-compmath.jku.at

Homepage:

<http://www.dk-compmath.jku.at>